Pedro Manuel Barbosa Mota

Licenciado em Química Aplicada - Perfil Química Aplicada

Dendrimer-based Report-Eradication Antineoplasic Machines

Dissertação para obtenção do Grau de Mestre em Bioquímica

Orientador: Doutor Vasco D.B. Bonifácio, IST-UL
Co-orientador: Doutora Jacinta Serpa, CEDOC-NMS

Júri:

Presidente: Prof. Doutor Carlos Alberto Gomes Salgueiro
Arguente: Doutor José António Pais Silva
Vogal: Doutor Vasco Daniel Bigas Bonifácio

FACULDADE DE CIÊNCIAS E TECNOLOGIA
UNIVERSIDADE NOVA DE LISBOA

Março 2018

Pedro Manuel Barbosa Mota

Licenciado em Química Aplicada - Perfil Química Aplicada

Dendrimer-based Report-Eradication Antineoplasic Machines

Dissertação para obtenção do Grau de Mestre em Bioquímica

Orientador: Doutor Vasco D.B. Bonifácio, IST-UL
Co-orientador: Doutora Jacinta Serpa, CEDOC-NMS

Júri:

Presidente: Prof. Doutor Carlos Alberto Gomes Salgueiro
Arguente: Doutor José António Pais Silva
Vogal: Doutor Vasco Daniel Bigas Bonifácio

Dendrimer-based Report-Eradication Antineoplasic Machines

Acknowledgments

First of all, I have to thank Dr. Vasco Bonifácio for his help and guidance through this thesis. Thank you for all the knowledge and expertise shared during this process. But most of all, I have to thank you for receiving me in the more difficult time of my academic journey.

I also would like to thank my co-supervisor, Dr. Jacinta Serpa, for accepting me on her laboratory and give me the opportunity to work in a clinical research environment.

Not forgetting by laboratory colleagues. I would like to thank Rita Pires for helping me all the time I needed. For all your patience and joy. To Adriana, Edgar and Carina as well, for turning the days in the laboratory more fun.

Thank you to my colleagues in IPO. To Sofia Nunes, thank you for all that you teach me and all the support during my period at IPO. To Cristiano, for all help you gave me to finish this thesis. To Inês, Cindi, Filipa, Clara and Patricia for making me feel welcome in the laboratory.

I would like to thank *La Familia* (Nuno, Ana and Carolina) for being with me through the masters. With you this wasn't so difficult.

To my colleagues, Gomes and Diogo, for being that friends that are always there.

To my all my friends, Duarte, Becas, BA, etc., for all the time we passed when I needed to relax and take my head off the thesis.

A special thanks to my girlfriend, for living all the good and bad stages during this thesis, and for taking care of me when I'm needed peace to write this thesis. This thesis would not be possible without you.

I would like to thank my brothers for all the strength and support and since the beginning. To Julio for all the drive and support in the bad days. "All goes way", you said. To César, for all the jokes and fun that you share with me.

To my cousin Nádia, for all the guidance she gave all the way.

To my mother and grandmother, for the sacrifice and inspiration.

Abstract

Polyurea (PURE) dendrimers are a versatile platform for cancer nanotheranostics. The aim of this study was to improve the therapeutic efficacy of carboplatin by a buthionine sulfoximine (BSO) triggered inhibition of glutathione synthesis. BSO nanodelivery was achieved by controlled release from an encapsulated formulation using a folate target polyurea dendrimer of generation four (BSO@PURE$_{G4}$-FA). Platinum-based anti-cancer drugs, such as cisplatin and carboplatin have been widely used in chemotherapy. In particular, carboplatins are used as standard chemotherapeutic in ovarian cancer, a silent killer, which is the most lethal gynecologic malignancy and the seventh most common cancer among women worldwide. However, carboplatin chemoresistance is a major problem and there is evidence that increased glutathione levels play an important role in the anticancer mechanism of action. Cell death assays using OVCAR3 (OSC) and ES2 (OCCC) ovarian cancer cell lines were used to determine the efficacy of BSO@PURE$_{G4}$-FA nanoformulations. Cytotoxicity data showed that the encapsulated drug, if compared with the free drug, improve the efficacy of BSO, by reduction of the IC_{50}, against both OVCAR3 (64-fold) and ES2 (146-fold) cell lines. The results showed that inhibition of glutathione synthesis improve the efficacy of carboplatin in both cell lines. In this study a new method for detection of BSO was also developed, based on UV detection upon BSO chemical derivatization.

Keywords: Ovarian cancer; Buthionine sulfoximine; Chemoresistance; Glutathione; Polyurea dendrimers; Controlled drug delivery

Resumo

Os dendrímeros de poliureia (PURE) são uma plataforma versátil para a teranóstica do cancro. O objectivo principal deste estudo foi melhorar a eficácia terapêutica da carboplatina, através da inibição da síntese de glutationa por ação da butionina sulfoximina (BSO). O estudo do efeito deste agente foi realizado efectuando a libertação controlada da sua forma encapsulada, usando um dendrímero de poliureia de quarta geração conjugado com ácido fólico como nanoveículo (BSO@PURE$_{G4}$-FA). Os fármacos de platina, como a cisplatina e a carboplatina, têm sido muito utilizados em quimioterapia. Em particular, as carboplatinas são utilizadas como terapia padrão do cancro do ovário, uma doença silenciosa altamente letal, e que é a sétima causa de morte em mulheres em todo o mundo. No entanto, a quimioresistência à carboplatina é um problema por solucionar, tendo estudos recentes comprovado que elevados níveis de glutationa tem um papel importante neste mecanismo. Neste trabalho foram realizados ensaios de morte celular usando linhas celulares do cancro do ovário, OVCAR3 e ES2, de modo a determinar a eficácia da nanoformulação de BSO desenvolvida. Os ensaios de citotoxicidade mostraram uma maior eficácia do BSO encapsulado, em comparação com a forma livre, tendo-se observado uma redução dramática no IC_{50} quer na linha OVCAR3 (64 vezes) quer na linha ES2 (146 vezes). Os resultados obtidos mostraram ainda que a inibição da síntese de glutationa aumenta a eficácia da carboplatina em ambas as linhas celulares. Neste estudo foi também desenvolvido um novo método, simples e rápido, de detecção do BSO por UV-Vis, após derivatização química.

Palavras-chave: Cancro do ovário; Butionina sulfoximina; Quimioresistência; Glutationa; Dendrímeros de poliureia; Libertação controlada de fármacos

Content

Figures

Tables

Abbreviations

AA – Antibiotic-antimycotic

ATCC – American Type Culture Collection

BSA – Bovine Serum Albumin

BSO – Buthionine Sulfoximine

DAPI – 4',6-diamidino-2-phenylindole

DCC – *N*,*N'*-dicyclohexylcarbodiimide

DMEM – Dulbecco's Modified Eagle Medium

DMSO – Dimethyl Sulfoxide

EDTA – Ethylenediaminetetraacetic Acid

EPR – Enhanced Permeability and Retention

EOC – Epithelial Ovarian Cancer

FA – Folic Acid

FBS – Fetal Bovine Serum

FIGO – International Federation of Gynecology and Obstetrics

FITC – Fluorescein Isothiocyanate

FLA – Fluorescein Anhydride

FR – Folate Receptor

GS – Glutathione Synthetase

γ-GCS – γ-Glutamylcysteine Synthetase

GSH – Glutathione

GSSG – Glutathione Disulfide

HEPES – 4-(2-hydroxyethyl)-1-piperezineethanesulfonic Acid

HPLC – High Performance Liquid Chromatography

IC_{50} – Half Maximal Inhibitory Concentration

MWCO – Molecular Weight Cut-Off

NHS – *N*-hydroxisuccinimide

NMR – Nuclear Magnetic Resonance

OCCC – Ovarian Clear Cell Carcinoma

OSC – High-grade Serous Carcinoma

PAMAM – Polyamidoamine

PBS – Phosphate Buffer Saline

PEG – Polyethylene Glycol

PI - Propidium Iodide

PPI – Poly(propylene imine)

PURE – Polyurea

ROS – Reactive Oxygen Species

TEA – Triethylamine

1. Introduction

1.1. Dendrimers in cancer nanotechnology

A dendrimer (from the greek *dendros*, meaning tree, and *meros*, meaning part) is a complex artificial nanoscale organic macromolecule. Dendrimers, like hyperbranched polymers, are build up around a central core molecule and have branched segments that grow exponentially in terms of end-group functionalities and molecular weight. They have a well-defined and highly structured layered three-dimensional architecture with low polydispersity and high functionality.

Dendrimers have attracted enormous attention in recent years. Their popularity stems from two major features: the ability for their chemical composition and molecular weight to be precisely regulated during their synthesis, and the potential for their peripheral functionalization to be controlled. The latter feature affects numerous properties that include chemical reactivity, solubility and photo-physical properties [1].

Dendrimers contain three distinct regions: the core, the branches and the surface (Fig. 1.1). The central core is covalently linked to layers of repeating units (generations). As the branches ramify from the central core, the structure becomes more dense and compact, leaving the core relatively bare of molecules. These internal cavities permit the encapsulation of molecules, essentially allowing the dendrimer to perform as a “nanoscopic” container [2]. A three-dimensional architecture, multifunctional surface, presence of internal cavities, and great monodispersity makes dendrimers excellent drugs carriers for use in nanoscale medical applications. Furthermore, as a result of their hydrophobic cavities they confer higher solubility to drugs [3].

The diminished size of nanoparticles (~20-200 nm) allow them to extravasate through tumors’ leaky vessels. Then, due to the lack of efficient lymphatic drainage, they are retained in the tumor tissue. This phenomenon, collectively termed Enhanced Permeability and Retention (EPR) effect, has been the basis for nanoparticles use in cancer therapy [4].

Considering the enormous potential applications of dendrimers, selectively functionalizing their periphery is of paramount importance. Amine terminated dendrimers have the ability for their surface to be functionalized via an amide bond. Of these, polyamidoamine (PAMAM), poly(propylene imine) (PPI) and polyamide have been the most investigated dendrimers, largely due to the fact of being commercially available.

The nature of the surface of these nanoparticles is a critical determinant for its *in vitro* and *in vivo* performance, as it affects how dendrimers interact with blood proteins, the

immune system and tumor tissues [5,6]. Hydrophilic polymers like polyethylene glycol (PEG) stand out as the most frequently used surface coating for nanoparticles [7]. PEGylation, using PEGs of different molecular weight (~2-20 kDa) creates a steric barrier on the nanoparticles surface, which delays and decreases plasma protein adsorption (opsonization) and subsequent immune clearance [8,9]. PEG's ability to hide nanoparticles from the immune system, known as *stealth* effect, increases the nanoparticles circulation time, which subsequently allows for a higher accumulation in the tumor [9,10].

Although PEG is efficient in extending nanoparticle circulation time, its presence on the nanoparticle surface interferes with their interaction with target cells. This problem is known as the *PEG dilemma* [11].

To overcome this problem, the surface of nanoparticles can be functionalized with cell/receptor-specific ligands. These ligands can recognize certain markers and receptors on the surface of cancer cells, interacting with them. This interaction enhances nanoparticle uptake in the tumor tissue via-receptor-mediated endocytosis [12,13]. Increased cellular uptake can lead to enhanced drug delivery and therapeutic efficacy, especially when the drug encapsulated into the nanoparticle acts on intracellular targets, or when cancer cells have drug efflux mechanisms [14,15].

Among used ligands, small molecular weight (<1 kDa) molecules such as folic acid (FA), galactose, estradiol and biotin are the most frequently used. This is due to the over-expression of their receptors several types of tumor cells, facilitating nanoparticles uptake [16–19].

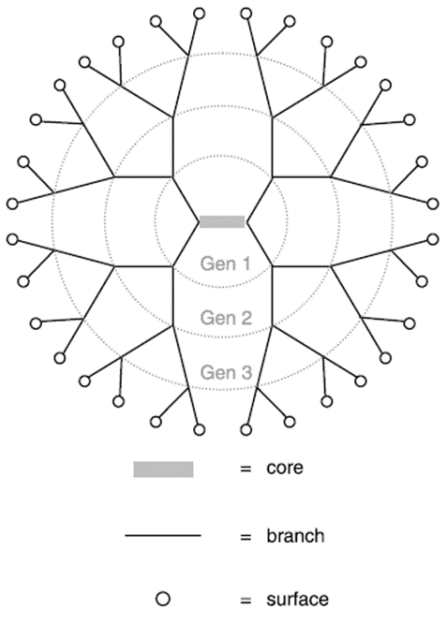

Figure 1.1 – Schematic representation of a third-generation dendrimer composed by the core, branch units and surface. Adapted from [1].

Dendrimers are used as drug nanocarriers in targeted therapy because they can offer both passive and active targeting abilities [20]. Passive tumor targeting is attributed to the EPR effect [20,21]. Active tumor targeting is achieved by conjugating ligands to the nanoparticle surface, thus enabling them to detect and bind specifically with the receptors overexpressed by cancer cells [22,23]. In addition, they can also improve the chemical stability of the encapsulated drug [24], enhance the cellular drug uptake [25,26], and potentially reduce multi-drug resistance [27,28]. PAMAM-type dendrimers are actually the most tested dendrimers as drug vectors, however their cytotoxicity is a major drawback.

A new class of amine-terminated polyurea (PURE) dendrimers has been recently reported [29]. PURE dendrimers (Fig. 1.2) are a new class of intrinsically fluorescent, biocompatible, pH responsive and biodegradable [30] polymers. Studies conducted on the first ($PURE_{G1}$) up to the fourth ($PURE_{G4}$) generation of PURE dendrimers have suggested that they are less cytotoxic than amine-terminated PAMAM dendrimer [29].

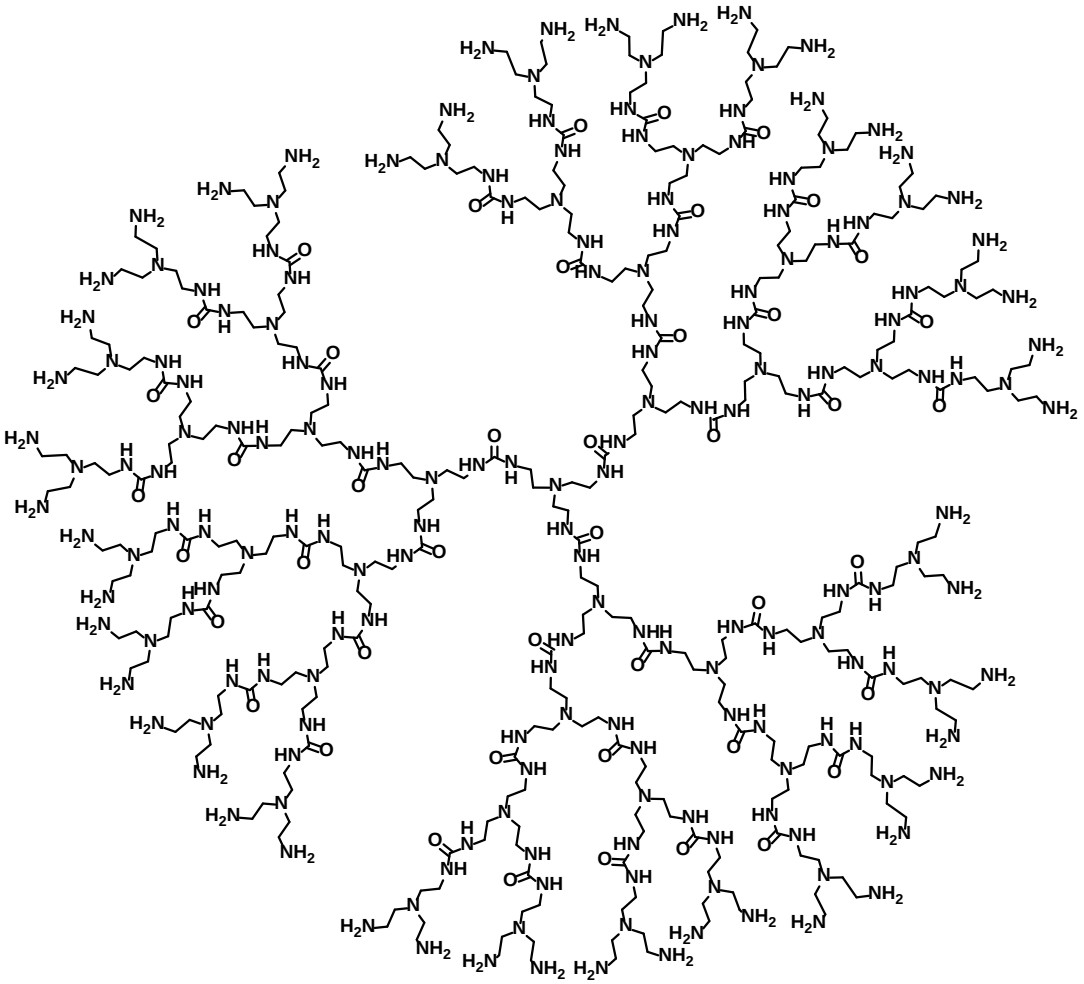

Figure 1.2 – Chemical structure of a polyurea (PURE) fourth-generation dendrimer ($PURE_{G4}$).

Moreover, PURE dendrimers have already demonstrated its potential as nanocarriers [31]. These family of dendrimers have shown promising results in the delivery of paclitaxel [32] and siRNA [33].

1.2. Ovarian cancer

Ovarian cancer is the most lethal gynecologic malignancy and the seventh most common cancer among women worldwide [34]. As reported by GLOBOCAN, in 2012 239,000 new cases were diagnosed and 152,000 deaths related to ovarian cancer occurred. Ovarian cancer is considered to be the eight most common cause of death from cancer in women [35]. Incidence rates are highest in developed countries, with rates in these areas being higher than 7.5 per 100,000 people, and lowest in Sub-Saharan Africa with rates below 5 per 100,000 people [35].

Poor outcomes in ovarian cancer can be attributed to a number of factors, including difficulties in early diagnosis, ease of metastasis, and because existing treatments are not effective enough [36]. Due to the absence of early warning symptoms, about 70% of ovarian cancer cases are diagnosed at an advanced stage and have a bad prognosis. Late-stage ovarian cancer is incurable in the majority of cases [37].

Adopting certain behaviors can lead to an increased risk of developing ovarian cancer, for example poor diet, a sedentary lifestyle, and reproductive factors, such as lower parity and higher age upon first birth. These factors have further increased the cancer burden in less economically developed countries. Due to population growth and aging, the global cancer burden is expected to grow [38].

Efforts at early detection and new therapeutic approaches to reduce mortality have been largely unsuccessful, because the origin and pathogenesis of epithelial ovarian cancer have long been investigated but still poorly understood [39].

Studies have suggested that epithelial ovarian cancer is not a single disease but a diverse group that can be classified based on distinct morphologic and molecular genetic features [39].

Ovarian cancer stages range from I through IV and are often described by the International Federation of Gynecology and Obstetrics (FIGO) staging system. In stage I ovarian cancer is confined to the ovaries [40]. In stage II ovarian cancer has metastasized to extraovarian organs. Stage II may also include curable tumors that have directly extended to adjacent organs but have not yet metastasized. By stage III most ovarian cancers have spread

along peritoneal surfaces involving both the pelvic and the abdominal peritoneum. High-grade serous carcinoma (OSC) is overall the most prevalent type ovarian cancer and is usually present in stage III [41]. Stage IV, present in 12 to 21% of patients [41], is defined as distant metastasis and includes patients with parenchymal liver or spleen metastases and extra-abdominal metastases.

1.2.1. Diagnosis and therapeutics

Early detection is defined as the early identification of cancer in patients who have symptoms of the disease. The objective of cancer early diagnosis is to identify the disease at the earliest possible opportunity and link diagnosis and treatment without delay. When done promptly, cancer may be detected at a potentially curable stage, improving survival chances and quality of life [42].

There are three key steps to early cancer diagnosis. These steps correspond to the standard patient-initiated health-seeking pathway across diseases: awareness and health-seeking, diagnosis and initiating treatment. The first step comprehends the period from detecting a bodily change, to identifying a reason to discuss the symptoms with a health-care practitioner, and finally to reaching the health facility for an assessment. The second step can be classified into three components: accurate clinical diagnosis, diagnostic testing and staging, and referral for treatment. Patients with suspicious findings for cancer should receive diagnostic tests, pathological confirmation, and staging studies at an appropriate diagnostic facility. Diagnosis is made mainly by detecting morphological changes and it is critical before starting cancer treatment [42].

Once diagnosis of cancer has been confirmed, the patient should receive staging examinations. The objective of staging is to assess whether and where to cancer may have spread. Accurate staging is essential for effective cancer treatment, because a patient with metastatic cancer requires different treatment than a person with localized cancer.

In the third step, the patient with cancer needs to be able to access high-quality and affordable treatment in a timely manner. The goal is to ensure that as many patients as possible initiate treatment within one month of the diagnosis being confirmed [43]. There is consistent evidence that early diagnosis of cancer, combined with accessible, affordable effective treatment, results in improvements in both the stage of cancer at presentation and mortality [44, 45].

While improving early diagnosis improves outcomes, not all cancer types benefit equally. Cancer that are common, that can be diagnosed at early stages from signs and symptoms, and

for which early treatment is known to improve the outcome, are generally those that benefit most from early diagnosis [43]. Some of them include breast, cervical, colorectal and oral cancers. Currently, no effective methods exist for the screening and early diagnosis of ovarian cancer [46].

When detected as an intra-ovarian disease, ovarian cancer has an excellent prognosis. However, because early detection methods are not sufficiently accurate the majority of ovarian cancer are detected late, at stage III or IV, which results in high fatality rates [47,48]. The major challenge of ovarian cancer is that early stage ovarian cancer is often asymptomatic and once symptoms appear the disease is often already advanced.

The standard treatment for ovarian cancer is maximal cytoreductive surgical debulking followed by a platinum-based chemotherapy. Confirmation of the diagnosis, as well as staging of the disease is performed during surgery [37]. According to the 2017 European Society of Gynecological Oncology ovarian cancer surgery guidelines, the aim of the frontline surgery is to achieve complete cytoreduction [49]. In advanced stages (III/IV), complete cytoreduction is often not possible. Patients with inoperable lesions are first treated with induction chemotherapy. Treatment outcome is assessed after the completion of first-line chemotherapy and the evaluation of response to the treatment is done based on imaging.

In chemotherapy, regimens containing platinum drugs have been the standard of care for almost 40 years worldwide. Platinum-based anti-cancer drugs, such as cisplatin and carboplatin have been widely used to treat various types of cancers clinically, including ovarian cancer [50–52].

Over the years, experts and research groups have explored different combinations of antitumor drugs in order to improve prognosis of ovarian cancer. Cisplatin has become established as an antitumor agent of major clinical importance since its introduction in the early 1970s [53]. In the early 1990, another turning point in the treatment of ovarian cancer was related to the discovery of paclitaxel. Paclitaxel acts by promoting microtubular assembly and stabilizes tubulin polymer formation and has great activity in epithelial ovarian cancer. However, the severe toxicity associated with cisplatin led to development of second generation compounds [54,55]. Carboplatin, a cisplatin analogue, is reported to have fewer marked side effects than cisplatin, particularly nausea, renal toxicity, hearing loss, and neuromuscular toxicities [55,56]. The carboplatin-paclitaxel combination is now considered an almost universal regimen in the management of epithelial ovarian cancer.

Platinum sensitivity, which is defined by a response to first-line platinum-based therapy, has been found to predict the response to subsequent retreatment with platinum-containing regimen. In general, patients which have their condition improve or have stable disease during

first-line treatment but relapse within one month are considered to be ‘platinum-refractory’. Patients who respond to primary treatment and relapse within six months are considered ‘platinum-resistant’, and patients who relapse more than six months after completion of initial therapy are characterized as ‘platinum sensitive’ [57]. Despite the activity of first-line chemotherapy, which gives response rates up to 80% in first line treatment, the majority of patients die of their recurrent disease [58].

Our team has described [59] the glutathione scavenger system as one of the responsible mechanisms for ovarian cancer chemoresistance. Testing buthionine sulfoximine (BSO) as an inhibitor of reduced glutathione (GSH) synthesis the *in vitro* and *in vivo* models showed that BSO sensitizes cancer cells and xenograft tumors to carboplatin. However, as GSH is crucial for the endogenous metabolic flow, the systemic inhibition of GSH synthesis would be devastating. This problem can be solved using targeted delivery approaches.

In conventional chemotherapy, therapeutic agents are distributed non-specifically throughout the body after intravenous injection. Therefore, they affect both malignant and normal cells. As a result, limited dose of drug reaches to tumor and healthy cells are exposed to the toxic chemotherapy drug [60]. Therefore, effectiveness of ovarian cancer chemotherapy may be strongly linked to the efficiency of drug delivery.

1.2.2. Role of glutathione in cancer chemoresistance

Glutathione is a tripeptide, γ-L-glutamyl-L-cysteinylglycine, present in all mammalian tissues, predominantly in the liver. It is the most abundant non-protein thiol that defends cells against oxidative stress. GSH is synthesized in the cytosol from its constituents’ amino acids: L-glutamate, L-cysteine, and L-glycine. Eukaryotic cells have three major reservoirs of GSH. Most of cellular GSH (80-85%) is present in the cytosol, 10-15% is in the mitochondria and a small percentage is in the endoplasmatic reticulum [61–63]. GSH exists in the thiol-reduced and the disulfide-oxidized (glutathione disulfide, GSSG) forms [64], being reduced GSH the most predominant form, accounting for over 98% of total glutathione [65–67].

1.2.3. Glutathione synthesis

The synthesis of GSH involves two ATP-requiring enzymatic steps (Fig. 1.3). The first step is the formation of γ-glutamylcysteine from glutamate and cysteine, catalyzed by γ-glutamylcysteine synthetase (γ-GCS). γ-GCS is a heterodimer composed by heavy (GCLC) and light (GCLM) subunits. The GCLC subunit catalyzes the synthesis of peptide γ-

glutamylcysteine and is feedback inhibited by GSH [68]. The GCLM subunit plays an important regulatory role increasing the affinity between glutamate and the GCLC subunit [69,70]. The second step in GSH synthesis is catalyzed by GSH synthetase (GS), composed of two identical subunits. GS does not undergo feedback inhibition by GSH [71].

The first step is considered the rate-limiting step of GSH biosynthesis, since the product catalyzed by γ-GCS is present at low concentration when GS is present [72]. This information is supported by *Grant et al.*, that observed that the overexpression of GS failed to increase GSH levels, whereas overexpression of γ-GCS increased GSH level [73].

In the GSH structure, the peptide bond linking glutamate and cysteine, is through the γ-carboxyl group of glutamate rather than the conventional α-carboxyl group. [74]. The only enzyme that can hydrolyze this bond is γ-glutamyltranspeptidase, which is only present on the external surface of certain cell types [75]. For this reason, GSH is resistant to intracellular degradation and is only metabolized extracellularly by cells that express γ-glutamyltranspeptidase. This allows for the released GSH to be broken down and for its constituent amino acids taken up by cells and reincorporated into GSH.

GSH has several vital physiological roles. It is the major cellular antioxidant, being crucial in maintaining the balance between oxidation and reduction. It is also important in cellular detoxification and is required in many steps of the immune response.

Reactive oxygen species (ROS) result from metabolism performed by all aerobic organisms. Highly active intermediates are formed, namely hydrogen peroxide and superoxide, which promote the production of ROS that in turn leads to cellular damage [76]. GSH provides protection against oxidative stress by serving as a substrate for the antioxidant enzymes glutathione peroxidase and phospholipid hydroperoxide GSH peroxidase [77] that convert peroxides into less harmful fatty acids, water and GSSG.

GSH is also able to protect cells against oxidative stress by non-enzymatic scavenging of ROS. Reduced GSH can directly scavenge radicals and peroxides via mixed disulfide formation, or upon oxidization of GSSG. There is evidence that a variety of ROS can result in GSSG formation and depletion of GSH in the short term [78]. Cells are highly sensitive to signals via changes in their environment. A vast number of cellular processes are affected by the redox state of the cell, in which GSH has a crucial role. Many signaling molecules are activated by GSH redox status, either directly, or indirectly through interaction with ROS. Molecules activated in this way are involved in a wide range of cellular pathways such as cellular proliferation, differentiation and morphogenesis.

GSH is required in many stages of the immune response. Intracellular GSH has been shown to modulate not only T-cell function, including the binding, internalization, and degradation of interleukin-2 [79], but also DNA synthesis [80]. GSH and other sulfhydryl compounds can also enhance cytotoxic T-cell activation, proliferation and differentiation [81]. Studies have shown not only that *in vivo* administration of GSH can activate cytotoxic T-cells, but also that depletion of intracellular GSH can inhibit the activation of lymphocytes, suppressing their cytotoxic functions and increasing susceptibility of the cell to radiation damage [82].

Cells are constantly being exposed to toxins which are damaging chemical substances. These include environmental pollutants, heavy metals and drug metabolites. The conjugation of toxins to GSH in mammalian cells is particularly important in the detoxification of electrophilic substances such as epoxides, alkenes, halides and heavy metals [64].

The GSH redox system plays a crucial role in the detoxification of numerous chemotherapeutic drugs. Overexpression of GSH confers resistance to tumor cells and often limits the efficacy of chemotherapy [67]. There is evidence to suggest that increased GSH levels play an important role in anticancer drug resistance [59]. Increased intracellular GSH has been shown to be associated with reduced drugs sensitivity of tumor cells. This occurs in cell lines with acquired or intrinsic resistance to certain anticancer drugs, particularly platinum salts [57,83,84]. GSH has also been shown to exert an inhibitory effect on cisplatin-DNA monoadduct formation [85]. This in turn results in a decrease in DNA damage and thereby drug-induced cell death.

1.2.4. Buthionine sulfoximine as an inhibitor of glutathione synthesis

Chemoresistance has been successfully circumvented with GSH reducing agents such as buthionine sulfoximine (BSO). BSO is a specific γ-glutamylcysteine inhibitor, blocking the rate-limiting step of GSH biosynthesis developed by Griffith and Meister [86].

There are a number of problems associated with the analysis of BSO in biological matrices. Firstly, BSO has a very low molar absorptivity, and the greatest UV absortion is at wavelengths below 200 nm. Therefore, it is difficult to detect with high performance liquid chromatography (HPLC) using UV absorbance. Also, BSO is a zwitterionic and highly polar molecule, making its extraction from biological matrices difficult [87].

BSO is also a chiral compound that has two isomers, L-buthionine-(*R*)-sulfoximine and L-buthionine-(*S*)-sulfoximine. Being a chiral drug we cannot exclude different interactions

with biological systems, thus leading to pharmacological discrimination by the two stereoisomers [88]. In the case of BSO, L-(*S)*-BSO has a considerably greater activity in the inhibition of γ-GCS than L-(*R)*-BSO in both cultured cells and in animals [89,90]. It has been used in many studies to demonstrate that a reduction in GSH sensitizes cell lines and animal models to drug treatment [59,91–93].

A number of research groups undertook phase I clinical studies to determine clinically whether BSO produced the desired biochemical end point of GSH depletion. In these preliminary studies, it was revealed that continuous infusion of BSO was relatively non-toxic and resulted in the depletion of tumor GSH in patients with advanced cancers, including ovarian cancer [94,95].

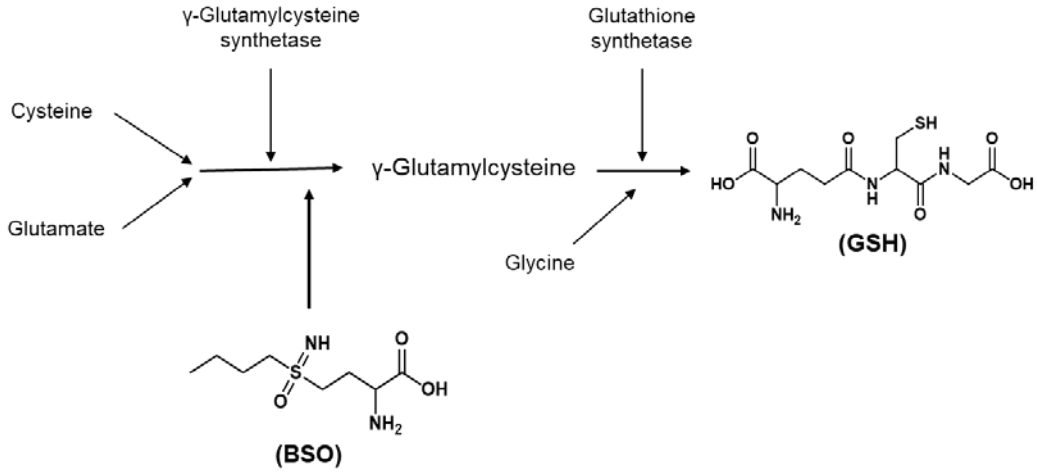

Figure 1.3 – Glutathione synthesis and buthionine sulfoximine (BSO) activity.

1.3. Purpose of the work

The main goal of this study is to increase the efficacy of carboplatin in ovarian cancer cells. Combining the drug delivery proprieties of PURE dendrimers and the inhibitory activity of BSO against GSH synthesis allowed the creation of complex therapeutic nanoparticles. GSH has been reported has one of the principal agents to chemoresistance, and modulation of its concentration could lead to more successful cancer treatments.

The use of nanoparticles in therapeutics is attracting much interest in the scientific community due to the improvement of drugs target and uptake. Increase the efficacy of chemotherapeutic agents and decrease the dose of adjuvant drugs was our big challenge.

2. Materials and methods

2.1. Materials

Different polyurea (PURE) dendrimer generations were synthesized following a reported supercritical-assisted polymerization methodology [29]. All chemicals and solvents were used as received without further purification. Fluorescein anhydride (FLA) was available in the host lab. Folic acid (FA) and *N*,*N*'-dicyclohexylcarbodiimide (DCC) (99% purity) were obtained from Alfa Aesar. Triethylamine (TEA) (≥ 99.5% purity), *N*-hydroxisuccinimide (NHS) (98% purity) and buthionine sulfoximine (BSO) (≥ 97% purity) were obtained from Sigma-Aldrich.

2.2. Preparation of BSO@PURE$_{G4}$-FA

2.2.1. Synthesis of FA-NHS

The synthesis of FA-NHS followed a reported protocol [95]. Typically, in a round bottom flask, 250.0 mg (0.5664 mmol) of FA was dissolved in DMSO (2.75 mL). After the addition of 130.8 mg (1.137 mmol) of NHS, 128.5 mg (0.6228 mmol) of DCC and 0.15 mL (1.082 mmol) of TEA the reaction was stirred at room temperature overnight in the dark. The product was precipitated with diethyl ether. After washing the precipitate three times with diethyl ether, and drying under vacuum, a yellow powder (263.4 mg) was obtained in 86.4% yield.

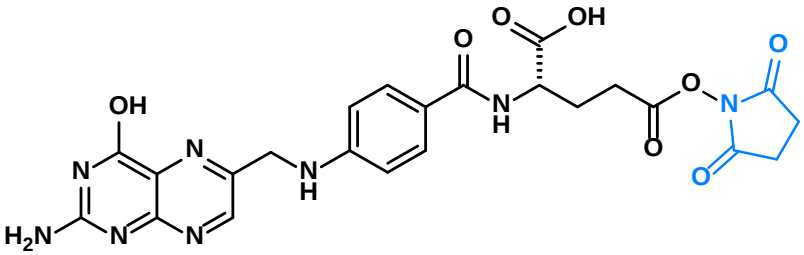

FA-NHS: ^{1}H NMR (400 MHz, DMSO-*d6*) δ (ppm): 8.64 (s, 1H), 7.63 (d, *J* = 8.0 Hz, 2H), 6.64 (d, *J* = 8.0 Hz, 2H), 4.49 (s, 2H), 4.28 (s, 1H), 2.54 (s, 4H), 2.29 (s, 1H), 2.03 (s, 1H), 1.93 (s, 1H). Yield: 86.4%.

2.2.2. Synthesis of PURE$_{Gn}$-FA

In a 50 mL bottom round flask, 100 mg (0.1633 mmol) of PURE$_{G1}$ dendrimer were dissolved in 5.0 mL of DMSO. To this solution, 162.54 mg (0.3018 mmol, 2 equiv.) of FA-NHS and 83.7 µL (0.6038 mmol, 4 equiv.) of TEA were added. The reaction was stirred at room temperature overnight in the dark. Next, TEA excess was removed on the rotary evaporator and diethyl ether was added. The obtained precipitate was then dried under vacuum. A yellow oil (182.2 mg) was obtained in quantitative yield. The same procedure was followed using polyurea dendrimers generations 4 (PURE$_{G4}$), 5 (PURE$_{G5}$) and 6 (PURE$_{G6}$). In the case of PURE$_{G6}$ dendrimer, the protocol was slightly modified, as follow: 200 mg (6.117 µmol) of PURE$_{G6}$ was reacted with 66.0 mg (0.1226 mmol, 20 equiv.) of FA-NHS and 34 µL (0.2454 mmol, 40 equiv.) of TEA.

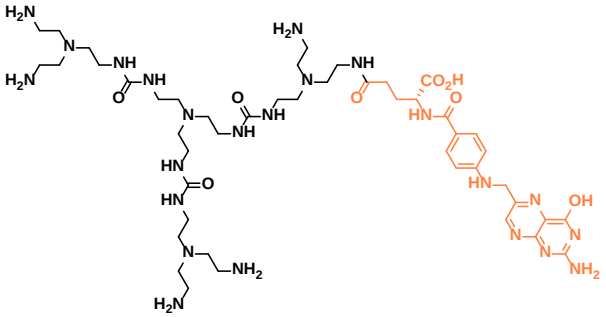

PURE$_{G1}$-FA: ^{1}H NMR (400 MHz, D_2O) δ (ppm): 8.64 (s, 1H), 7.69 (br, 2H), 6.84 (br, 2H), 4.61 (s, 4H), 3.36-3.06 (m, 12 H), 3.04-2.47 (m, 42 H). Quantitative yield.

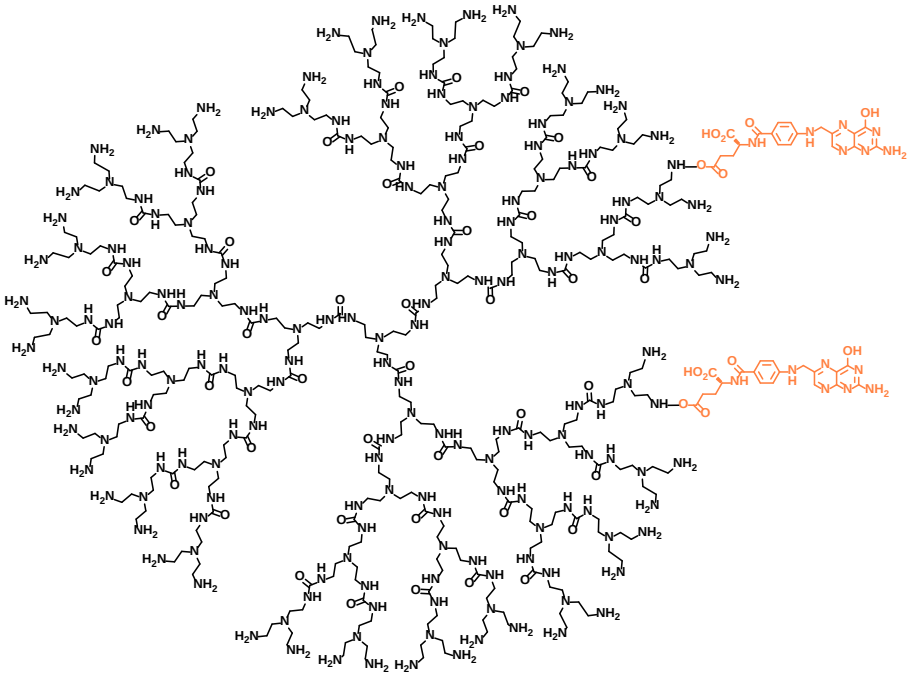

PURE$_{G4}$-FA: ^{1}H NMR (400 MHz, D_2O) δ (ppm): 8.64 (s, 2H), 7.70 (br, 4H), 6.86 (d, *J* = 8.0 Hz, 4H), 4.61 (s, 2H), 3.54-3.00 (m, 180H), 2.96-2.40 (m, 462H). Yield: 93.9%.

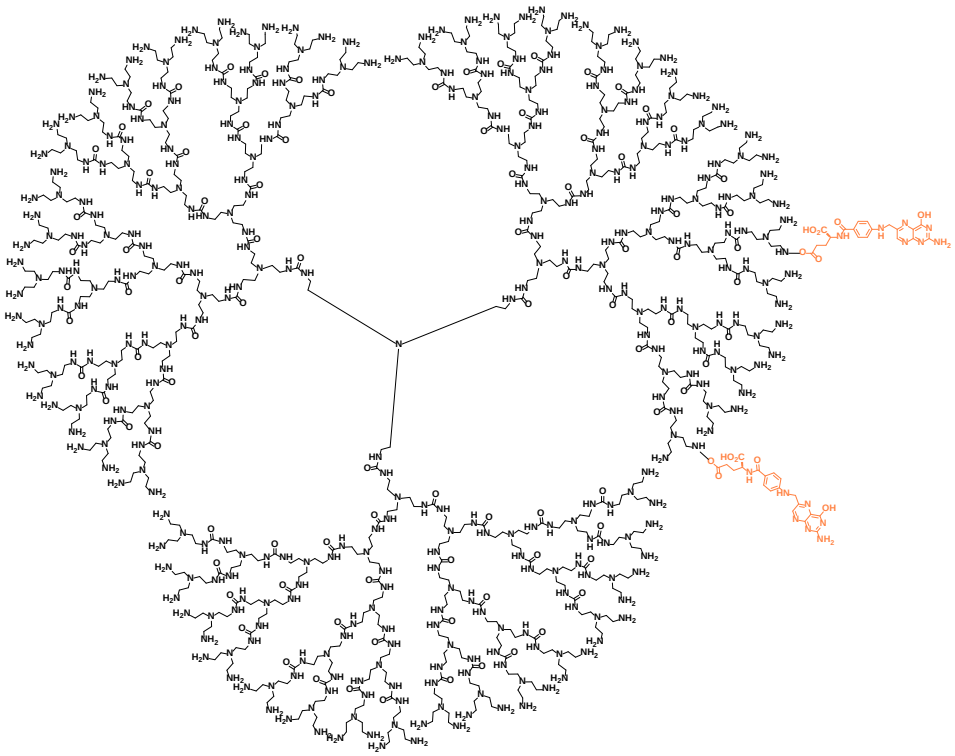

PURE$_{G5}$-FA: ^{1}H NMR (400 MHz, D_2O) δ (ppm): 8.64 (s, 2H), 7.70 (br, 4H), 6.84 (br, 2H), 3.42-3.06 (m, 372H), 3.04-2.38 (m, 1233H). Quantitative yield.

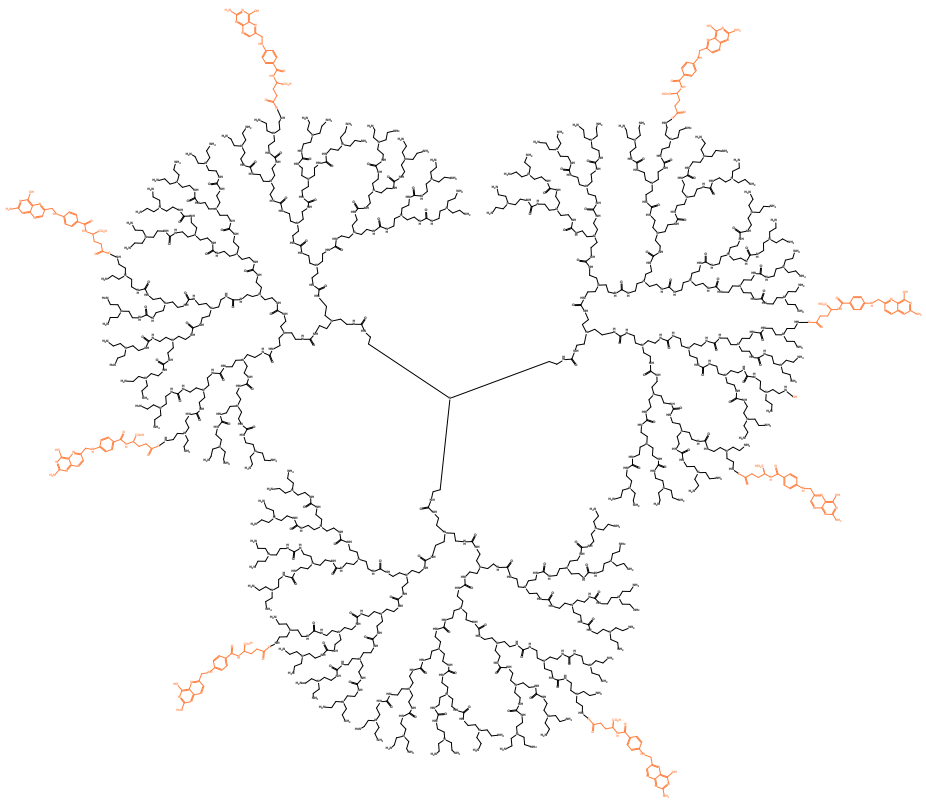

PURE$_{G6}$-FA: ^{1}H NMR (400 MHz, D_2O) δ (ppm): 8.63 (s, 8H), 7.69 (br, 16H), 6.82 (br, 16H), 4.61 (s, 16H), 3.24-2.44 (m, 756H), 3.01-2.42 (m, 2253H). Quantitative yield.

2.2.3. Encapsulation of BSO in PURE$_{G4}$-FA

In a vial, 78.0 mg (8.90 μmol) of PURE$_{G4}$-FA was dissolved in 20 mL of methanol. Then, 21.6 mg (0.0972 mmol) of BSO was added and the mixture vigorously stirred. The encapsulation occurred at room temperature, in the dark, for 48 hours. Afterwards, no BSO on suspension was observed and the product was purified by dialysis (MWCO 100-500 Da). After evaporation of the solution, the product was dried under vacuum and characterized by ^{1}H NMR. The amount of BSO loaded into the dendrimer was determined by ^{1}H NMR.

BSO@PURE$_{G4}$-FA: ^{1}H NMR (300 MHz, D_2O) δ (ppm): 8.60 (s, 2H), 7.63 (br, 4H), 6.78 (br, 4H), 3.62 (s, 16H), 3.44-3.07 (m, 180H), 3.06-2.40 (m, 462H), 1.76 (m, 32H), 1.45 (q, *J*= 6.0 Hz, 30H), 0.92 (t, *J* = 6.0 Hz, 48H).

2.2.4. Encapsulation of FLA in PURE$_{G4}$-FA

PURE$_{G4}$-FA dendrimer was loaded with fluorescein anhydride (FLA). In a vial, 5.3 mg (0.0131 mmol) of FLA was dissolved in 1 mL of distilled water. To this solution, 56.6 mg (6.46 μmol) of PURE$_{G4}$-FA was added. The encapsulation occurred at room temperature, in the dark and under stirring. After 2 days, the product was purified by dialysis (MWCO 100-500) and characterized by ^{1}H NMR. The signals of FLA in NMR sample were not detected due to low concentration (*ca.* 0.9 mg FLA/10 mg FLA@PUREG4-FA). However, FLA was detected by fluorescence spectroscopy.

FLA@PURE$_{G4}$-FA: ^{1}H NMR (300 MHz, D_2O) δ (ppm): 8.60 (s, 2H), 7.61 (br, 4H), 6.80 (br, 4H), 3.60-2.90 (m, 180H), 2.85-2.33 (m, 462H).

2.2.5. Drug release study

BSO release studies were performed at 37 °C in sodium phosphate buffer medium (PBS, pH 7.4). First, 6.3 mg of BSO@PURE$_{G4}$-FA were dispersed in 1 mL of medium and placed in a SnakeSkin™ dialysis membrane (MWCO 3500 Da). The dialysis bag was then immersed in 60 mL of release medium and kept in a at constant temperature with stirring. Samples (1 mL) were periodically collected and replaced by the same volume of fresh medium. The amount of

BSO released was determined by UV/Vis spectroscopy. The release of BSO from the dendrimers was obtained in triplicate.

2.2.6. Quantification of BSO by UV/Vis spectroscopy

Since BSO has a very low molar absorptivity and the maximum absorption wavelength is below 200 nm [87], a new detection protocol was developed. Following a reported protocol [96], BSO was derivatized in order to be able to be detected by UV/Vis. The quantification of BSO was performed by adding to the samples 300 µL of catechol 2.25 mM, followed by sodium periodate 6.75 mM. After 60 sec the absorption of the BSO derivative (503 nm) was measured in a PerkinElmer Lambda 25 UV/Vis Spectrometer with a slit width of 5 nm at a scan rate of 240 nm min^{-1} at 25 °C. For the calibration curve, standard solutions of BSO were prepared in the concentration range of 0.1-150 µM and processed using the same protocol. A good correlation coefficient (R^2= 0.997) was achieved (Appendix I).

2.3. *In vitro* studies

2.3.1. Cell lines

Cell lines from OCCC (ES2; CRL-1978), OSC (OVCAR-3; HTB-161) and HaCaT (HB-241) were obtained from American Type Culture Collection (ATCC). Cells were maintained at 37 °C in a humidified 5% CO_2 atmosphere. Cells were cultured in DMEM 1× (41965-039, Gibco, Life Technologies) containing 4.5 g/L of D-glucose and 0.58 g/L of L-glutamine supplemented with 10% FBS (S 0615, Merck), 1% antibiotic-antimycotic (AA) (P06-07300, PAN Biotech).

Both ovarian cancer cell lines were seeded in 25 cm^3 T-flasks until confluence was obtained. Cell culture media was exchanged every 2 days. Afterward, cell culture media was rejected, cells were washed with PBS 1× and 5 mL of trypsin-EDTA (0.25%; 25200056, Gibco, Life Technologies) was added to total cells loss of adherence. After a few minutes, trypsin was neutralized with the same volume of DMEM 1× with 10% FBS and cells were centrifuged during 2 minutes at 1200 rpm. Then, cell culture media was rejected and the pellet was resuspended in 6 mL of DMEM sup culture media. The cell suspension was transferred to 75 cm^3 T-flasks and incubated in a humified atmosphere of 5% CO_2 at 37 ºC. HaCaT (HB-241) cells were use has negative control in fluorescence microscopy.

2.3.2. Cell death assay

2.3.2.1. Determination of IC_{50} of BSO and BSO@$PURE_{G4}$-FA

Cells (1×10^5 cells/well) were seeded in 24-well plates and cultured overnight in control condition (DMEM 1×, 4.5 g/L of D-glucose, 0.58 g/L of L-glutamine, 10% FBS and 1% AA). Several concentrations of BSO (between 0.05-80 mM in OVCAR3 and 0.05-120 mM in ES2) and BSO@$PURE_{G4}$-FA (between 1 and 400 µM) in culture medium were tested, for 24 hours. To certificate that $PURE_{G4}$-FA has no cytoxicity to the cell lines in study, the same procedure was followed. The concentration corresponding to the equivalent number of nanoparticles used in the assay with BSO@$PURE_{G4}$-FA was used. Cell death analysis was performed by flow cytometry. The assay was performed at least in 3 biological replicates.

2.3.2.2. Cell death analysis by flow cytometry

Cells were collected to 1.5 mL eppendorf. First, the supernatant of each well, containing dead cells. Then, after cells detachment with trypsin-EDTA (as described above) the living cells were collected to the same eppendorf. Cells were harvested by centrifugation at 1200 rpm for 3 min, and incubated with 0.5 µL annexin V-Alexa Fluor® 488 (640906, BioLegend) in 100 µL annexin V binding buffer 1× (10 mM HEPES (pH 7.4), 0.14 M sodium chloride (NaCl), 2.5 mM calcium chloride ($CaCl_2$)) and incubated at room temperature and in the dark for 15 min. After incubation, samples were rinsed with 0.1% (w/v) BSA (A9647, Sigma) in PBS 1× and centrifuged at 1200 rpm for 3 min. Cells were suspended in 200 µL of annexin V binding buffer 1× and 2.5 µL of Propidium Iodide (PI) (50 µg/mL). Acquisition was performed in a FACScalibur (Becton Dickinson). Data were analysed with FlowJo software. The assay was performed at least in 3 biological replicates.

2.3.2.3. Combined anticancer activity of BSO and carboplatin

Cells (1×10^5 cells/well) were seeded in 24-well plates overnight and exposed to the previous conditions combined with carboplatin 25 µg/ml. Cells were collected after 24 hours of BSO@$PURE_{G4}$-FA exposure combined with 24 hours of carboplatin exposure. Cell death analysis was performed by flow cytometry. The assay was performed at least in 3 biological replicates.

2.3.3. Cellular nanoparticles uptake assays

2.3.3.1. Flow cytometry

Cells were cultured (1×10^5 cells/well) overnight in 24-well plates. Then, incubated with several concentrations of FLA@PURE$_{G4}$-FA (between 5 - 1000 µM) prepared in DMEM 1x for 24 hours. Only viable cells were taken for the analysis. Cells were washed with PBS 1x, and 150 µL of trypsin was added to detached with trypsin-EDTA, as described above. Cells were collected to 1.5 mL eppendorf. Cells were harvested by centrifugation at 1200 rpm for 3 min and washed twice with PBS 1×. Cells were suspended in 200 µL of PBS 1×. Acquisition was performed in a FACScalibur (Becton Dickinson). Data were analysed with FlowJo software.

2.3.3.2. Fluorescence microscopic analysis

Cells OVCAR3 and HaCaT (negative control) were grown on glass slides with a 0.2% gelatin coating, in control conditions until 80% of confluence and then incubated with FLA@PURE$_{G4}$-FA nanoparticles for 24 hours. Cells were fixed in 2% paraformaldehyde for 15 min at 4 °C. The slides were mounted in VECTASHIELD media with DAPI (4′-6-diamidino-2-phenylindole) (Vector Labs) and examined by standard fluorescence microscopy using an Axio Imager.Z1 microscope (Zeiss). Images were acquired and processed with CytoVision® software.

3. Results

3.1. Preparation and characterization of BSO@PURE$_{G4}$-FA

With the objective of targeting PURE$_{Gn}$ dendrimers with folate, the first step was the synthesis of the folate intermediate FA-NHS, which was obtained in 86.4% yield. Folate conjugation at the dendrimer's surface was successful achieved by reaction of FA-NHS with amine-terminated PURE dendrimers. All the products of this synthesis were analyzed by ^{1}H-NMR. For generations 1, 4 and 5, two molecules of FA per PURE dendrimer were found to be conjugated to the surface. In the case of PURE$_{G6}$-FA dendrimer 8 molecules of FA were incorporated. Since PURE$_{G6}$ is the dendrimer of higher molecular weight (32,698 g/mol), with 192 amine groups at its surface, we used an excess (20 equivalents, instead of 2) of FA-NHS, which resulted in a higher number of folates at the surface. Analyzing the ^{1}H-NMR spectra of PURE$_{Gn}$-FA, three peaks above 6.0 ppm are observed. These peaks are attributed to the aromatic protons of the FA (Appendix II) and were used to quantify the number of conjugated FA molecules per PURE dendrimer. Of all PURE$_{Gn}$-FA dendrimers synthetized, due to time constraints, only PURE$_{G4}$-FA was used in encapsulation assays with BSO. The quantification of encapsulated BSO was performed by ^{1}H-NMR. By analysis of the ^{1}H-NMR spectra of BSO@PUREG4-FA, we found that 16 molecules of BSO were loaded into the PURE$_{G4}$-FA dendrimer.

3.2. Drug release study

Figure 3.1 shows the BSO release profile from BSO@PURE$_{G4}$-FA at pH 7.4. The release profile was followed for 24 hours, and the results indicate a burst release of BSO in the first hours. After 1 hour, around 60% of the drug loaded was released to the medium, reaching a plateau after 3 hours. After 24 hours, 90% of BSO was released, meaning that a residual amount of BSO is trapped inside PURE$_{G4}$-FA dendrimer in this period of time.

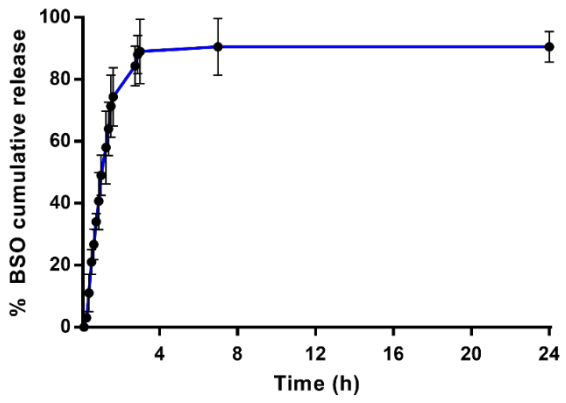

Figure 3.1 – *In vitro* drug release profile of buthionine sulfoximine (BSO) encapsulated into PURE$_{G4}$-FA dendrimer at pH 7.4.

3.3. Cell death assays

In order to determine the IC_{50} of BSO cell viability assays were performed in two different ovarian cancer cell lines, OSC (OVCAR3) and OCCC (ES2). Cells were exposed to different concentrations of BSO for 24 h. After cell death analysis, the results (Fig. 3.2) showed a higher IC_{50} for ES2 than OVCAR3 cells, 56.23 mM and 38.49 mM respectively. So, ES2 cells were more resistance to BSO than OVCAR3 cells and this is clearly seen by the fact that the maximum cell death is ES2 is 60% whereas in OVCAR3 is about 80%.

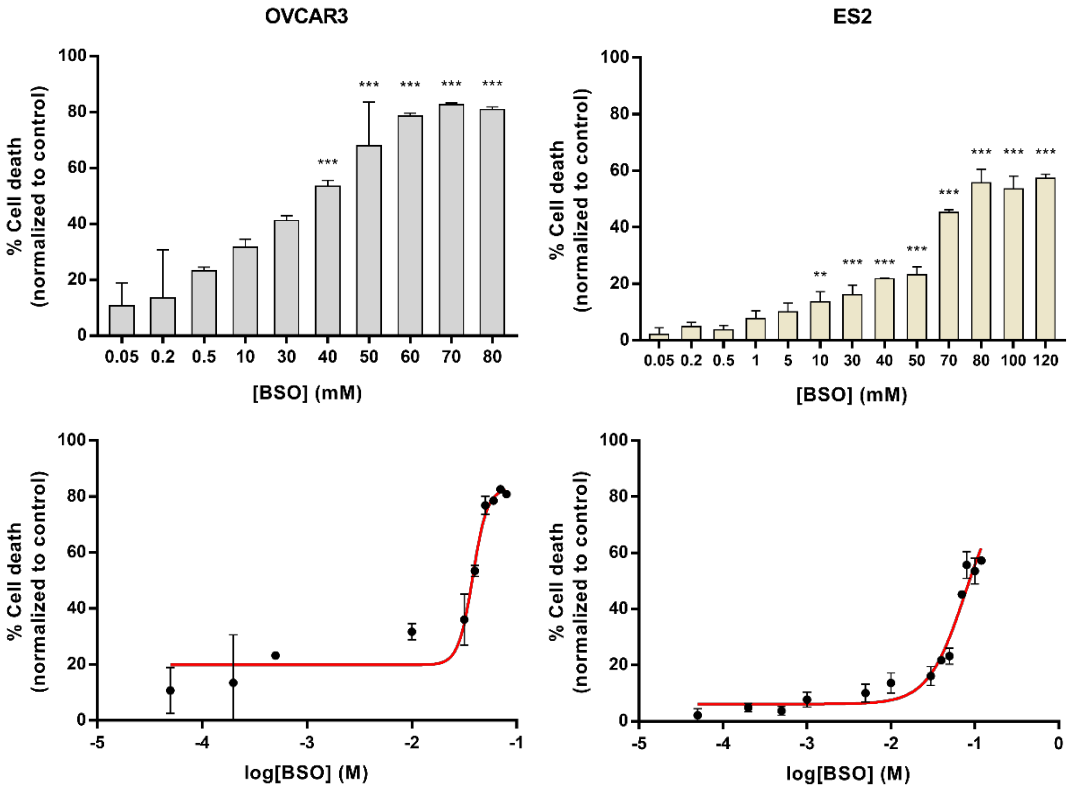

Figure 3.2 – Cell death evaluation by flow cytometry, annexin V, and PI staining. OVCAR3 and ES2 cells were treated with different concentrations of BSO for 24 h. Dose-response curve used in the calculation of IC_{50} values. Error bars represent standard deviation; statistical significance **p<0.01, ***p<0.001.

Afterwards, BSO@PURE$_{G4}$-FA was used in the same conditions to determine the IC_{50}. The concentrations used in this assay was regarding the number of BSO molecules inside the dendrimer. The results (Fig. 3.3) indicate a considerably IC_{50} values decrease in comparison to free BSO. The IC_{50} value obtained was 0.562 mM and 0.384 mM, for OVCAR3 and ES2, respectively. This result indicates that BSO is delivered in a more effective way when is encapsulated in the nanoparticle than when it is delivered freely to the cells.

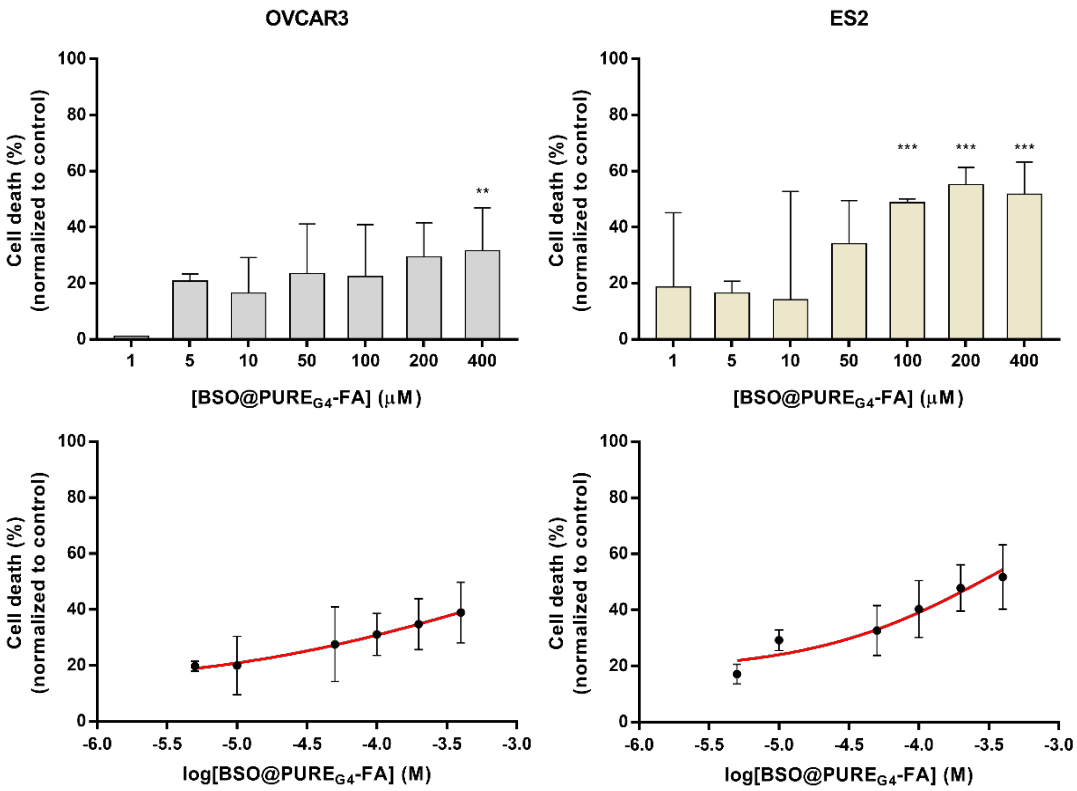

Figure 3.3 – Cell death evaluation by flow cytometry, annexin V, and PI staining. OVCAR3 and ES2 cells were treated with different concentrations of BSO@PURE$_{G4}$-FA for 24 h. Dose-response curve used in the calculation of IC_{50} values. Error bars represent standard deviation; statistical significance **p<0.01, ***p<0.001.

To certificate that the death observed was due the action of encapsulated BSO and not from the PURE$_{G4}$-FA nanoparticles itself, the same assay was performed using only PURE$_{G4}$-FA (empty nanoparticles). In this assay (Fig. 3.4), it was used concentrations of PURE$_{G4}$-FA dendrimer that correspond to same number of nanoparticles for each concentration in the BSO@PURE$_{G4}$-FA assay. In OVCAR3 cells, nanoparticles didn't affect viability of cells, with the percentage of cell death never reaching 10%. ES2 cells it seems to be more sensible to the nanoparticles than OVCAR3. When the concentration of PURE$_{G4}$-FA reaches 70 µg/mL, considerably cells deaths is observed (~30%).

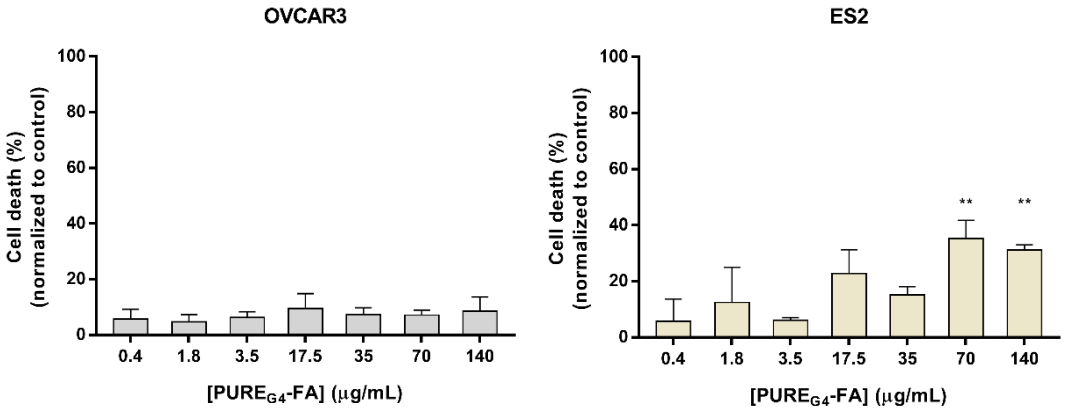

Figure 3.4 – Cell death evaluation by flow cytometry, annexin V, and PI staining. OVCAR3 and ES2 cells were treated with different concentrations of PURE$_{G4}$-FA for 24 h. Error bars represent standard deviation; statistical significance **p<0.01.

3.4. Combined anticancer activity of BSO and carboplatin

A combined strategy of BSO and carboplatin was used (Fig. 3.5). After 24 hours of exposure with BSO encapsulated into PURE$_{G4}$-FA nanoparticles, new media supplemented with 25 μg/mL of carboplatin was added to cells for 24 hours. For this assay it was chosen concentrations that caused approximately 30% of cell death, from the cell death assays performed with BSO@PURE$_{G4}$-FA nanoparticles. These concentrations were chosen with the objective evaluate the activity of carboplatin after the inhibithion of glutathione synthesis.

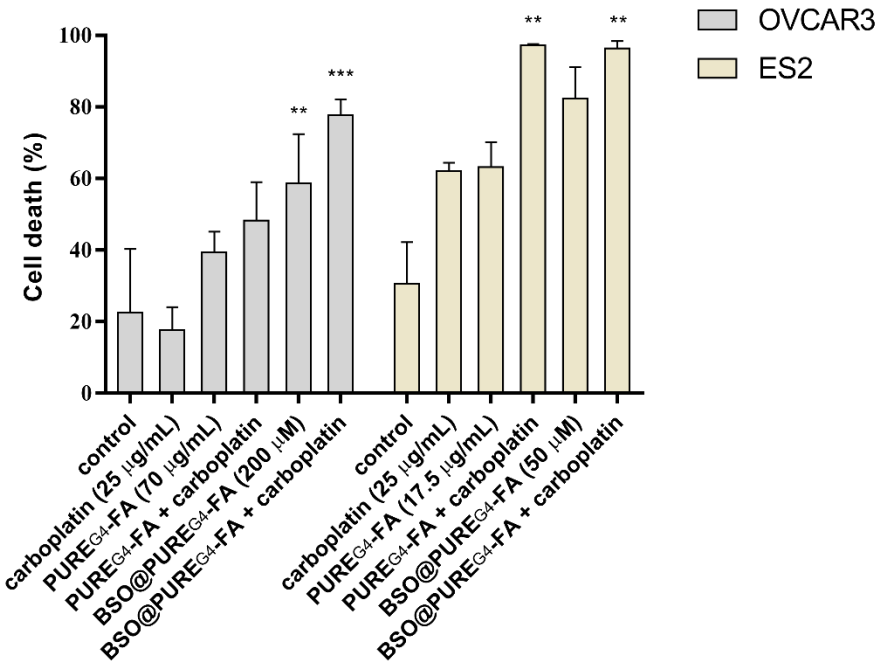

Figure 3.5 – Cell death evaluation by flow cytometry, annexin V, and PI staining. OVCAR3 and ES2 cells were treated with BSO@PURE$_{G4}$-FA and PURE$_{G4}$-FA for 24 h. Later, cells were either exposed to carboplatin (25 μg/mL) for 24 h. Error bars represent standard deviation; statistical significance **p<0.01, ***p<0.001.

The results indicated that combined activity of these two compounds is very effective in OVCAR3 and ES2 cell lines. The carboplatin itself didn't show any effect in OVCAR3, whereas in ES2 cells the carboplatin causes a considerable cell death. However, when carboplatin was used after the exposure to BSO, the effect of carboplatin was significant. This result shows the importance of GSH levels in chemoresistance to carboplatin.

3.5. Cellular nanoparticles uptake assays

To confirm that nanoparticles were internalized by the cells, nanoparticle uptake was analyzed by flow cytometry and fluorescence microscopic. Green fluorescent nanoparticles (FLA@ $PURE_{G4}$-FA) were formulated by encapsulating FLA into $PURE_{G4}$-FA dendrimer. After a 24-hour incubation with FLA@$PURE_{G4}$-FA, viable cells were collected and the fluorescence was measured by flow cytometry (Fig. 3.6).

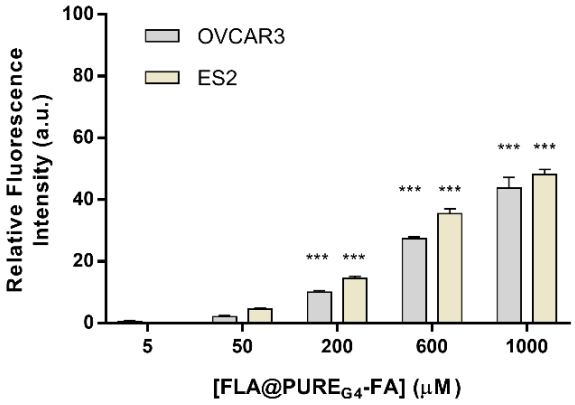

Figure 3.6 – Fluorescence signal of OVCAR3 and ES2 cells. Relative fluorescence intensity after incubation with different FLA@$PURE_{G4}$-FA concentrations for 24h. Error bars represent standard deviation; statistical significance ***p<0.001.

The results show that fluorescence of cells increase with greater FLA@$PURE_{G4}$-FA concentration. This result indicate that nanoparticles are being internalized by the cells. The encapsulation happens in a similar way in both OVCAR3 and ES2 cell lines.

Then, the encapsulation of nanoparticles was confirmed by fluorescence microscopic (Fig. 3.7). Exposing the FLA@$PURE_{G4}$-FA nanoparticles for 24 hours, a green fluorescence (emission from the FLA molecule), was observed inside the cells. HaCaT cells, a non-cancerous cell line, were used as negative control. The difference observe on the uptake of nanoparticles between both cell lines is clear. Unfortunately, it was not possible to perform this assay using the ES2 cell line.

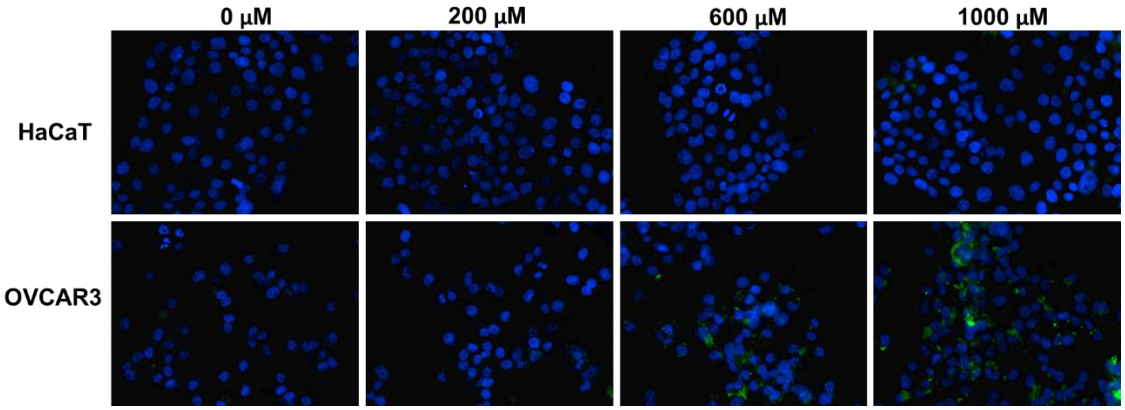

Figure 3.7 – Cellular uptake of FLA@PURE$_{G4}$-FA nanoparticles evaluated by fluorescence microscopy. OVCAR3 and HaCaT cells were treated with medium (control) and increasing concentrations of FLA@PURE$_{G4}$-FA for 24 h.

4. Discussion

In the present study, we aimed to develop a folate-targeted drug delivery system for the therapy of chemoresistant ovarian cancer. Therefore, two different types of histological *in vitro* models were studied, one representing a highly chemoresistant type (OCCC) [97] and the other being the most frequent type (OSC) [41].

From the analysis of the BSO release profile from the $PURE_{G4}$-FA nanoparticles we found that a burst release occurs in the first hours (Fig. 3.1). This release is generally observed when this system is used and may be explained by its the highly polarity [87], in opposition to the hydrophobic core of PURE dendrimers. Our study was performed at 37 °C under physiological conditions (pH 7.4). However, when the nanoparticles are up taken by the cancer cells via endocytosis an acidic environment is present [98]. Is known that PURE dendrimers have the ability to expand its structure when exposed to low pH, as a result of amine groups protonation [29]. This effect is the result of a greater molecular charge that result in charge-charge repulsions between the dendrimer branches [99]. Other studies also point to higher drug release profile at low pH [100,101]. Therefore, in more acidic media (e.g. cancer cells) the release of BSO is expected to be higher than the one observed at pH 7.4.

The detecting and quantification of BSO is a problematic issue. Due to a very low molar absorptivity (and $\lambda_{máx}$ below 200 nm), in order to know the release profile of encapsulated BSO, a new detection method was developed (Fig. 4.1). Is known from literature [96] that ortho phenols (e.g. catechol) react with sodium periodate to give *o*-quinones. This reaction is fast, and the formed *o*-quinones are highly reactive colored intermediates (absorption bands *ca.* 390 nm) Formed *o*-quinones, due to its electron deficient character, easily undergo nucleophilic attack [102]. Since the derivatization reaction is time dependent, thus affecting the absorbance intensity, all the triplicate data points were rigorously collected with the same time of reaction (60 sec.), using a chronometer.

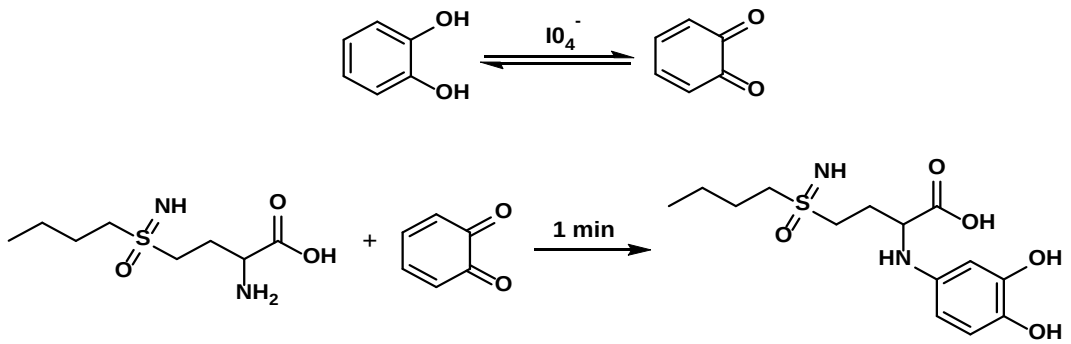

Figure 4.1 – Reaction of formation of *o*-quinone by catechol oxidation (top) and reaction that leads to formation of a possible colored BSO intermediate (bottom).

The reaction between *o*-quinone (prepared by oxidation of catechol with sodium periodate) and BSO results in a red solution with a maximum absorption at 503 nm. Figure 4.1 shows a possible chemical structure for the intermediate formed in this reaction.

In order to clarify the derivatization mechanism, the reaction was performed in a NMR tube and followed by ^{1}H (Fig. 4.2) and ^{13}C-NMR (Appendix III). By ^{1}H-NMR analysis we were able to follow all reaction steps. To catechol in D_2O (Fig. 4.2A), sodium periodate was added and *o*-quinone was formed (Fig. 4.2B). Then BSO was added (dissolved in D_2O) and the spectra recorded within periods of 10 min., till no more changes in the spectra were observed (total time 50 min.).

The formed product was not isolated, but the ^{13}C-NMR spectrum (Fig. 4.3) showed a downshift of the carbon signals, especially the ones found in the region 49-54 ppm, when compared with the BSO spectrum. The higher downshift was observed for the carbon around 53 ppm, which is the carbon linked to the BSO primary amine [103]. Based on this data, we may conclude that the formed BSO derivative results from the reaction between of *o*-quinone and the primary amine of BSO.

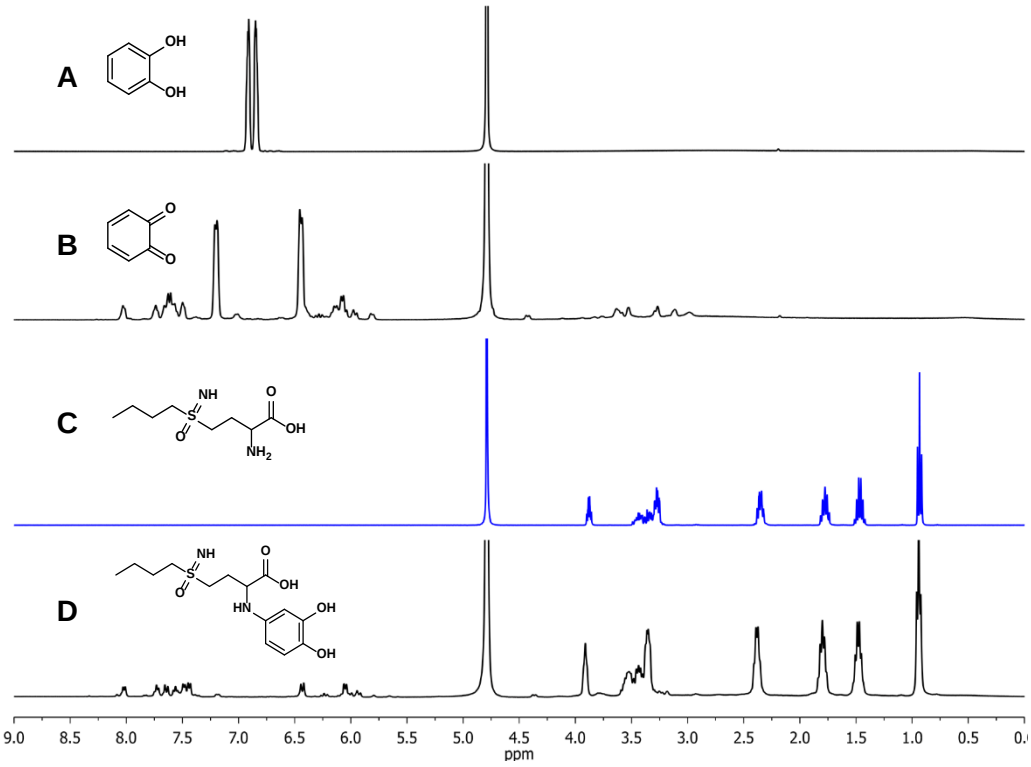

Figure 4.2 – ^{1}H-NMR spectra of the BSO derivatization reaction. Comparative spectrum of (A) catechol, (B) *o*-quinone, (C) BSO and (D) final BSO derivative. NMR spectrum recorded in D_2O.

In 1987, Duff and Murrill developed a method for detection of BSO by HPLC, after derivatization with *o*-phthaladehyde [104]. However, this analytical method has limitations.

Because of the instability of the *o*-phthaladehyde derivative at room temperature, each sample was prepared immediately prior to injection onto the HPLC column. Additionally, the internal standard required a fluorescence detector in addition to the UV detector used for the *o*-phthaladehyde. Later, in 1991, Campbell *et al.* developed an alternative method producing a more stable derivative, by using phenylisothiocyanate [105]. This reagent reacts readily with primary and secondary aminoacids, producing a stable derivative that strongly absorbs UV light at 254 nm, but makes use of phenylisothiocyanate, which is a highly toxic reagent.

During our study we developed a new BSO detection method, which in comparison with the one available provides a simple and fast analysis using non-toxic reagents, through UV-Vis measurement, thus avoiding HPLC.

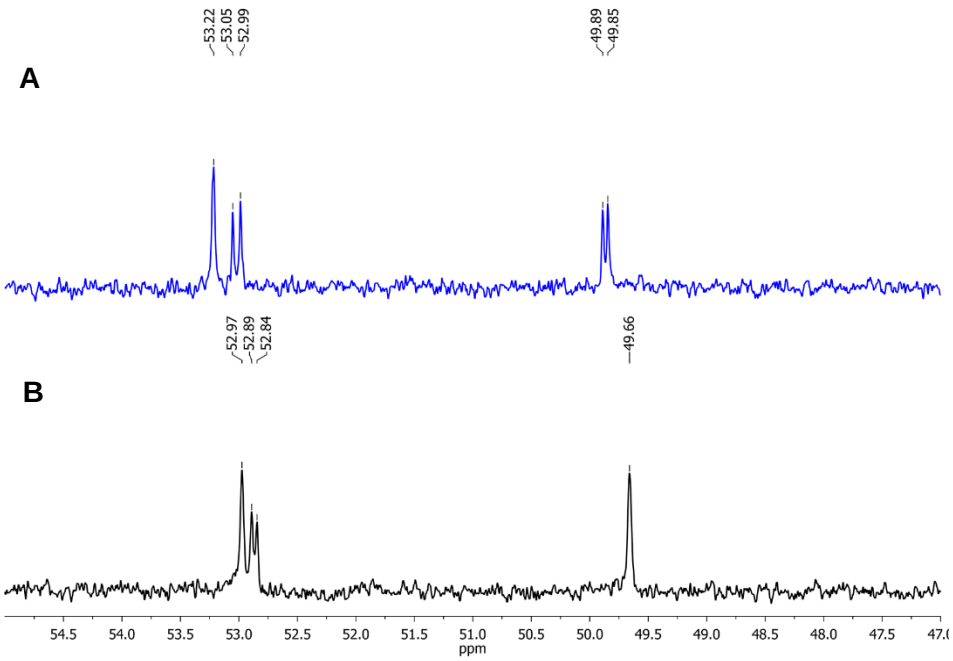

Figure 4.3 – ^{13}C-NMR amplified spectra of the BSO derivatization reaction. Comparative spectrum of (A) BSO and (B) BSO derivative.

The IC_{50} of BSO was determined for the OVCAR3 (38.2 mM) and the ES2 (56.2 mM) cell lines. In order to enhance its delivery to the cells, BSO was then encapsulated in $PURE_{G4}$-FA (BSO@$PURE_{G4}$-FA). As expected, the formulation of BSO@$PURE_{G4}$-FA decreased the IC_{50} of BSO, to 0.562 and 0.384 mM, for OVCAR3 and ES2 cell lines respectively. This means a 68-fold decrease of IC_{50} in OVCAR3 cells and a more remarkably 146-fold decrease in ES2 cells (Table 4.1). However, higher concentrations of BSO are needed in the assay with ES2, in order to reach the plateau of death and get a more accurate IC_{50}. According to a previous study reported by our team, the ES2 cell line present higher levels of GSH comparing

to OVCAR3 [59]. This finding can be responsible for the higher resistance of ES2 cells to BSO when delivered freely to the cells, showing a higher 1.47-fold IC_{50} than OVCAR3.This decreasing IC_{50} effect of PURE dendrimers was already reported in early studies. By encapsulation of paclitaxel in $PURE_{G4}OEtOx_{48}$ and in $PURE_{G4}OMeOx_{48}$ a 100-fold IC_{50} decrease was evaluated [32].

Table 4.1 – Calculated IC_{50} values of BSO and BSO@$PURE_{G4}$-FA after 24 hours exposure to ovarian cancer cell lines.

	IC_{50} (mM)		
Cell lines	**BSO**	**BSO@$PURE_{G4}$-FA**	**Reduction Factor**
OVCAR3 (OSC)	38.2	0.562	68.0
ES2 (OCCC)	56.2	0.384	146.4

Higher concentrations of BSO@$PURE_{G4}$-FA nanoparticles couldn't be used. As cell deaths was being evaluated, higher concentration creates a ratio problem between the number of cells and nanoparticles. This problem interferes in the cell death evaluation as nanoparticles were being detected by the cytometer.

The PURE dendrimer used in the *in vitro* studies, $PURE_{G4}$, show a lower cytotoxicity in the concentration range used. The non-cytotoxic profile of $PURE_{G4}$ has been early reported [29]. However, ES2 cells indicate some sensibility concerning the $PUGE_{G4}$-FA dendrimer.

Fluorescein anhydride (FLA) (Fig. 4.4) was successfully encapsulated into $PURE_{G4}$ dendrimers. This molecule is an analog of commercial fluorescein isothiocyanate (FITC) and was synthetized in our laboratory (unpublished data). Due to the lack of the isothiocyanate group, FLA is a less reactive fluorophore, if compared with FITC. However, this lower reactivity enables it encapsulation or surface decoration, an advantage over FTIC, which can only be used in surface targeting. FLA@$PURE_{G4}$-FA were internalized by both ovarian cancer cell lines, OVCAR3 and ES2, demonstrating an efficient and similar uptake of the nanoparticles. Fluorescence microscopy analysis indicate that uptake of this folate targeted nanoparticle does not occur equally in all cells types. The spontaneously immortalized human epithelial cell line, HaCaT, was used as model for the *in vitro* nanoparticle uptake by healthy cells. This non-tumoral cell line have low expression of folate receptors [106]. In comparison with OVCAR3, the uptake in these cells was very low (Fig. 3.7).

With this finding the importance of folate targeting is shown. Folic acid is essential for cell functioning, fast cell division and growth [107]. Folate receptor (FR) is known to be upregulated in a variety of human cancerous cells and among the three FR isoforms. FRα is the most widely expressed with very low levels in normal tissues, but high expression levels in many tumours [108], including the malignancies of the ovary [109]. The level of FR also appears to increase as the stage of the cancer increases [110,111]. FA is an ideal ligand for FR because of its high affinity ($K_d = 10^{-10}$ M), stability, and compatibility with both organic and aqueous solvents [111-113]. Moreover, the ligand is readily internalized into cells through receptor mediated endocytosis with non-immunogenicity [114]. These characteristics make FA an excellent agent for specific FR detection, drug delivery and cancer therapy [115–117]. For these reasons, folate targeting has been extensively used as recognition moiety in many conjugates [117].

The fluorescence microscopy images showed that nanoparticles are localized in the cytosol. This finding suggests that after endocytosis, nanoparticles may deliver BSO in the cytosol where the GSH is predominately found [54].

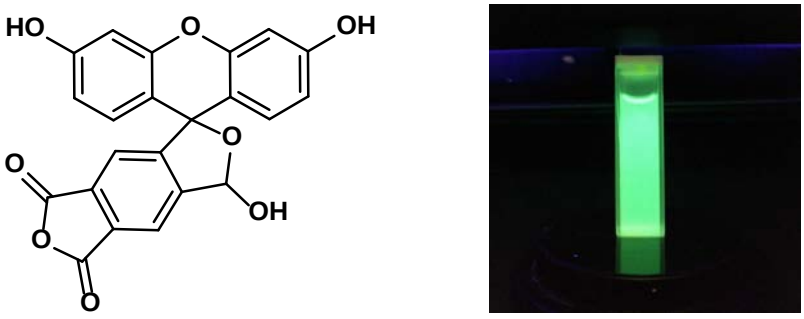

Figure 4.4 – Structure of fluorescein anhydride (FLA) and photograph of a quartz cell containing an aqueous solution of FLA excited by an UV lamp (λ_{ex}= 365 nm).

Inhibiting GSH synthesis with a 24-hour BSO exposure, leads to a complete depletion of GSH in cells [59]. The combination of low concentration of BSO@PURE$_{G4}$-FA and carboplatin resulted in high levels of cell death in both ovarian cancer cell lines. Delivering BSO specifically to cancer cells enables a reduction of the concentration of BSO applied. Carboplatin reacts promptly with highly nucleophilic sulfur-containing molecules [59], thus a higher concentration of GSH will be able to capture carboplatin. By decreasing the pool of GSH, carboplatin can bind to DNA, and cause cell death.

Our study paved the way for future experimental approaches in the course to validate PURE$_{G4}$-FA as a platform for drug nanodelivery in ovarian cancer. These nanoparticles can

be applied in a pre-sensitizing approach to cytotoxic drugs with BSO or in direct delivery of other types of chemotherapeutic agents. Currently, more experiments are ongoing to verify the higher specificity of $PURE_{G4}$-FA to ovarian cancer cells and also $PURE_{G4}$-FA direct cytotoxic effects in normal cells. Hence, more cell lines from ovarian carcinomas and cell lines with different origins (from normal tissues and cancer) will be tested.

5. Conclusions and future work

In summary, we report the behavior of PURE dendrimers, a new class of intrinsically fluorescent, biocompatible and pH responsive nanoparticles, that can be used as an efficient platform for BSO delivery. The ability of this smart materials to cross the cell membrane was clarified. Our results also indicate that $PURE_{G4}$ dendrimers effectively deliver BSO to cells and can efficiently deplete the GSH levels. Moreover, $PURE_{G4}$-FA show low cytotoxicity in the studied concentration range. The high efficacy of BSO delivery combined to the absence of cytotoxicity may be explored as a novel strategy in cancer therapeutics.

Future work will relay in the use of PURE dendrimers of higher generation, namely $PURE_{G5}$ and $PURE_{G6}$, which possess higher loading capacity. Additionally, more cell lines from ovarian carcinomas and cell lines with different origins (from normal tissues and cancer) will be tested. Finally, *in vivo* studies are also needed to validate the use of PURE dendrimers as reliable drug delivery system.

6. Bibliography

1. Trinchi A., Muster TH. A review of surface functionalized amine terminated dendrimers for application in biological and molecular sensing. Supramol Chem. 2007;19(7):431–45. DOI: 10.1080/10610270601120363

2. Johan F.G.A. Jansen, Ellen M.M. de Brabander-van den Berg EWM. Encapsulation of Guest Molecules into a Dendritic Box. Am Asssociation Adv Sci. 1994;266 (5188):1226–9. DOI: 10.1126/science.266.5188.1226

3. Baker J., Majoros I. Dendrimer-Based Nanomedicine. 2008. 332-335 p. Available from: https://apps.webofknowledge.com/full_record.do?product=UA&search_mode=GeneralSearch&qid=2&SID=Y2KIffKYeB8dcTMVbql&page=1&doc=6

4. Nichols JW, Bae YH. EPR: Evidence and fallacy. J Control Release. 2014;190:451–64. DOI: 10.1016/j.jconrel.2014.03.057

5. Yang Q, Lai SK. Anti-PEG immunity: Emergence, characteristics, and unaddressed questions. Wiley Interdiscip Rev Nanomedicine Nanobiotechnology. 2015;7(5):655–77. DOI: 10.1002/wnan.1339

6. Lundqvist M, Stigler J, Elia G, Lynch I, Cedervall T, Dawson KA. Nanoparticle size and surface properties determine the protein corona with possible implications for biological impacts. Proc Natl Acad Sci. 2008;105(38):14265–70. DOI: 10.1073/pnas.0805135105

7. Kumari A, Yadav SK, Yadav SC. Biodegradable polymeric nanoparticles based drug delivery systems. Vol. 75, Colloids and Surfaces B: Biointerfaces. 2010. p. 1–18. DOI: 10.1016/j.colsurfb.2009.09.001

8. Rabanel JM, Hildgen P, Banquy X. Assessment of PEG on polymeric particles surface, a key step in drug carrier translation. Vol. 185, Journal of Controlled Release. 2014. p. 71–87. DOI: 10.1016/j.jconrel.2014.04.017

9. Suk JS, Xu Q, Kim N, Hanes J, Ensign LM. PEGylation as a strategy for improving nanoparticle-based drug and gene delivery. Vol. 99, Advanced Drug Delivery Reviews. 2016. p. 28–51. DOI: 10.1016/j.addr.2015.09.012

10. Amoozgar Z, Yeo Y. Recent advances in stealth coating of nanoparticle drug delivery systems. Wiley Interdiscip Rev Nanomedicine Nanobiotechnology. 2012;4(2):219–33. DOI: 10.1002/wnan.1157

11. Hatakeyama H, Akita H, Harashima H. A multifunctional envelope type nano device (MEND) for gene delivery to tumours based on the EPR effect: A strategy for overcoming the PEG dilemma. Vol. 63, Advanced Drug Delivery Reviews. 2011. p. 152–60. DOI: 10.1016/j.addr.2010.09.001

12. Ding H Ming, Ma Y Qiang. Role of physicochemical properties of coating ligands in receptor-mediated endocytosis of nanoparticles. Biomaterials. 2012;33(23):5798–802. DOI: 10.1016/j.biomaterials.2012.04.055

13. Field LD, Delehanty JB, Chen Y, Medintz IL. Peptides for specifically targeting nanoparticles to cellular organelles: Quo vadis ? Acc Chem Res. 2015;48(5):1380–90. DOI: 10.1021/ar500449v

14. Duncan R, Richardson SCW. Endocytosis and intracellular trafficking as gateways for nanomedicine delivery: Opportunities and challenges. Mol Pharm. 2012;9(9):2380–402. DOI: 10.1021/mp300293n

15. Palakurthi S, Yellepeddi VK, Vangara KK. Recent trends in cancer drug resistance

reversal strategies using nanoparticles. Expert Opin Drug Deliv. 2012;9(3):287–301. DOI: 10.1517/17425247.2012.665365

16. Li M, Tang Z, Zhang Y, Lv S, Li Q, Chen X. Targeted delivery of cisplatin by LHRH-peptide conjugated dextran nanoparticles suppresses breast cancer growth and metastasis. Acta Biomater. 2015;18:132–43. DOI: 10.1016/j.actbio.2015.02.022

17. Jain S, Spandana G, Agrawal AK, Kushwah V, Thanki K. Enhanced Antitumor Efficacy and Reduced Toxicity of Docetaxel Loaded Estradiol Functionalized Stealth Polymeric Nanoparticles. Mol Pharm. 2015;12(11):3871–84. DOI: 10.1021/acs.molpharmaceut.5b00281

18. Ren WX, Han J, Uhm S, Jang YJ, Kang C, Kim J-H, et al. Recent development of biotin conjugation in biological imaging, sensing, and target delivery. Chem Commun. 2015;51(52):10403–18. DOI: 10.1039/c5cc03075g

19. Brannon-Peppas L, Blanchette JO. Nanoparticle and targeted systems for cancer therapy. Adv Drug Deliv Rev. 2012;64:206–12. DOI: 10.1016/j.addr.2004.02.014

20. Langer R. Drug delivery and targeting. Vol. 392, Nature. 1998. p. 5–10.

21. Davis ME, Chen Z, Shin DM. Nanoparticle therapeutics: An emerging treatment modality for cancer. Vol. 7, Nature Reviews Drug Discovery. 2008. p. 771–82. DOI: 10.1038/nrd2614

22. Byrne JD, Betancourt T, Brannon-Peppas L. Active targeting schemes for nanoparticle systems in cancer therapeutics. Vol. 60, Advanced Drug Delivery Reviews. 2008. p. 1615–26. DOI: 10.1016/j.addr.2008.08.005

23. V.J. Yao *et al.* Ligand-targeted theranostic nanomedicines against cancer. Vol. 240, Journal of Controlled Release. 2016. p.267–286. DOI: 10.1016/j.jconrel.2016.01.002

24. Ganta S, Devalapally H, Shahiwala A, Amiji M. A review of stimuli-responsive nanocarriers for drug and gene delivery. Vol. 126, Journal of Controlled Release. 2008. p. 187–204. DOI: 10.1016/j.jconrel.2007.12.017

25. Yonezawa A, Masuda S, Yokoo S, Katsura T, Inui K. Cisplatin and Oxaliplatin, but Not Carboplatin and Nedaplatin, Are Substrates for Human Organic Cation Transporters (SLC22A1-3 and Multidrug and Toxin Extrusion Family). J Pharmacol Exp Ther. 2006;319(2):879–86. DOI: 10.1124/jpet.106.110346

26. Los G, Verdegaal E, Noteborn HPJM, Ruevekamp M, de Graeff A, Meesters EW, *et al.* Cellular pharmacokinetics of carboplatin and cisplatin in relation to their cytotoxic action. Biochem Pharmacol. 1991;42(2):357–63.

27. Emilienne Soma C, Dubernet C, Bentolila D, Benita S, Couvreur P. Reversion of multidrug resistance by co-encapsulation of doxorubicin and cyclosporin A in polyalkylcyanoacrylate nanoparticles. Biomaterials. 2000;21(1):1–7.

28. Wang F, Wang YC, Dou S, Xiong MH, Sun TM, Wang J. Doxorubicin-tethered responsive gold nanoparticles facilitate intracellular drug delivery for overcoming multidrug resistance in cancer cells. ACS Nano. 2011;5(5):3679–92. DOI: 10.1021/nn200007z

29. Restani RB, Morgado PI, Ribeiro MP, Correia IJ, Aguiar-Ricardo A, Bonifácio VDB. Biocompatible polyurea dendrimers with pH-dependent fluorescence. Angew Chemie - Int Ed. 2012;51(21):5162–5. DOI: 10.1002/anie.201200362

30. Pires RF, Moro A, Lourenço A, Lima JC, Casimiro T, Bonifácio VDB. Molecular Weight Determination by Luminescent Chemo–enzymatics. ChemistrySelect. 2016;1(21):6818–

22. DOI: 10.1002/slct.201601301

31. Restani RB, Silva AS, Pires RF, Cabral R, Correia IJ, Casimiro T, *et al*. Nano-in-Micro POxylated Polyurea Dendrimers and Chitosan Dry Powder Formulations for Pulmonary Delivery. Part Part Syst Charact. 2016;33(11):851–8. DOI: 10.1002/ppsc.201600123

32. Restani RB, Conde J, Pires RF, Martins P, Fernandes AR, Baptista P V., *et al*. POxylated Polyurea Dendrimers: Smart Core-Shell Vectors with IC_{50}Lowering Capacity. Macromol Biosci. 2015;15(8):1045–51. DOI: 10.1002/mabi.201500131

33. Restani RB, Conde J, Baptista P V., Cidade MT, Bragança AM, Morgado J, et al. Polyurea dendrimer for efficient cytosolic siRNA delivery. RSC Adv. 2014;4(97):54872–8. DOI: 10.1039/C4RA09603G

34. Kim A, Ueda Y, Naka T, Enomoto T. Therapeutic strategies in epithelial ovarian cancer. J Exp Clin Cancer Res. 2012;31(1):14. DOI: 10.1186/1756-9966-31-14

35. Ferlay J, Soerjomataram I I, Dikshit R, Eser S, Mathers C, Rebelo M, et al. Cancer incidence and mortality worldwide: sources, methods and major patterns in GLOBOCAN 2012. Int J Cancer. 2015;136(5):E359-386. DOI: 10.1002/ijc.29210

36. Jayson GC, Kohn EC, Kitchener HC, Ledermann JA. Ovarian cancer. Lancet. 2014;384(9951):1376–88. DOI: 10.1016/S0140-6736(13)62146-7

37. Cortez AJ, Tudrej P, Kujawa KA, Lisowska KM. Advances in ovarian cancer therapy. Cancer Chemother Pharmacol. 2018;81(1):17–38. DOI: 10.1007/s00280-017-3501-8

38. Torre LA, Bray F, Siegel RL, Ferlay J, Lortet-tieulent J, Jemal A. Global Cancer Statistics, 2012. CA a cancer J Clin. 2015;65(2):87–108. DOI: 10.3322/caac.21262

39. Kurman R, Shih I. The Origin and pathogenesis of epithelial ovarian cancer-a proposed unifying theory. Am J Surg Pathol. 2010;34(3):433–43. DOI: 10.1097/PAS.0b013e3181cf3d79

40. Prat J, Committee F. International Journal of Gynecology and Obstetrics Staging classi fi cation for cancer of the ovary , fallopian tube , and peritoneum. Int J Gynecol Obstet. 2013;124:1–5. DOI: 10.1016/j.ijgo.2013.10.001

41. Heintz AP, Odicino F, Maisonneuve P, Beller U, Benedet JL, Creasman WT, *et al*. Carcinoma of the ovary. Int J Gynaecol Obstet Off organ Int Fed Gynaecol Obstet. 2003;66(2):184–90.

42. World Health Organization. Guide to cancer early diagnosis. 2017. Available from: http://www.who.int/cancer/publications/cancer_early_diagnosis/en/

43. World Health Organization . Cancer Control: Knowledge into Action: WHO Guide for Effective Programmes: Module 3: Early Detection. 2007;50. Available from: https://www.ncbi.nlm.nih.gov/books/NBK195408/

44. World Health Organization. National Cancer Control Programmes. Natl cancer Control Program Policies Manag Guid. 2002;180. Available from: http://www.who.int/cancer/publications/nccp2002/en/

45. Pontén J, Adami HO, Bergström R, Dillner J, Friberg LG, Gustafsson L, et al. Strategies for global control of cervical cancer. Int J Cancer. 1995;60(1):1–26.

46. Huang Z, Yan H, Chavan D, Yuan Z, Yang X, Zhang Y, et al. Effective treatment of a patient with stage IV ovarian cancer: A case report. Oncol Lett. 2018;15(1):588–91. DOI: 10.3892/ol.2017.7285

47. Belki K. The Challenge of Ovarian Cancer : Steps Toward Early Detection Through

Advanced Signal Processing in Magnetic Resonance Spectroscopy. 2017;517–25. Available from: https://www.ima.org.il/MedicineIMAJ/viewarticle.aspx?year=2017&month=08&page=517

48. Narod S. Can advanced-stage ovarian cancer be cured? Nat Rev Clin Oncol. 2016;13(4):255–61. DOI: 10.1038/nrclinonc.2015.224

49. III-IV S, Surgery OC. Quality Indicators Complete report.

50. Go RS, Adjei AA. Review of the comparative pharmacology and clinical activity of cisplatin and carboplatin. J Clin Oncol. 1999;17(1):409–22. DOI: 10.1200/JCO.1999.17.1.409

51. Rosenberg B. Platinum Complexes for the Treatment of Cancer: Why the Search Goes On. Cisplatin Chem Biochem a Lead Anticancer Drug. 2006;188(July):1–27. DOI: 10.1002/9783906390420.ch1

52. Wheate NJ, Walker S, Craig GE, Oun R. The status of platinum anticancer drugs in the clinic and in clinical trials. Dalt Trans. 2010;39(35):8113. DOI: 10.1039/c0dt00292e

53. Rosenberg B. Cisplatin: Its History and Possible Mechanisms of Action. Cisplatin. 1980. 9-20 p. DOI: 10.1016/B978-0-12-565050-2.50006-1

54. Wilkinson R, Cox PJ, Jones M, Harrap KR. Selection of potential second generation platinum compounds. Biochimie. 1978;60(9):851–7. DOI: 10.1016/S0300-9084(78)80569-0

55. Cleare MJ, Hydes PC, Malerbi BW, Watkins DM. Anti-tumour platinum complexes : relationships between chemical properties and activity. Biochimie. 1978;60(9):835–50. DOI: 10.1016/S0300-9084(78)80568-9

56. Calvert AH, Harland SJ, Newell DR, Siddik ZH, Jones AC, McElwain TJ, *et al*. Early clinical studies with cis-diammine-1,1-cyclobutane dicarboxylate platinum II. Cancer Chemother Pharmacol. 1982;9(3):140–7. DOI: 10.1007/BF00257742

57. Markman M, Reichman B, Hakes T, Jones W, Lewis JL, Rubin S, *et al*. Responses to second-line cisplatin-based intraperitoneal therapy in ovarian cancer: Influence of a prior response to intravenous cisplatin. J Clin Oncol. 1991;9(10):1801–5. DOI: 10.1200/JCO.1991.9.10.1801

58. Rubin SC, Randall TC, Armstrong KA, Chi DS, Hoskins WJ. Ten-year follow-up of ovarian cancer patients after second-look laparotomy with negative findings. Obstet Gynecol. 1999;93(1):21–4. DOI: 10.1016/S0029-7844(98)00334-2

59. Lopes-Coelho F, Gouveia-Fernandes S, Gonçalves LG, Nunes C, Faustino I, Silva F, *et al*. HNF1β drives glutathione (GSH) synthesis underlying intrinsic carboplatin resistance of ovarian clear cell carcinoma (OCCC). Tumor Biol. 2016;37(4):4813–29. DOI: 10.1007/s13277-015-4290-5

60. Vanneman M, Dranoff G. Combining immunotherapy and targeted therapies in cancer treatment. Nat Rev Cancer. 2012;12(4):237–51. DOI: 10.1038/nrc3237

61. Meredith MJ, Reed DJ. Status of the mitochondrial pool of glutathione in the isolated hepatocyte. J Biol Chem. 1982;257(7):3747–53.

62. Hwang C, Sinskey A, Lodish H. Oxidized redox state of glutathione in the endoplasmic reticulum. Science. 1992;257(5076):1496–1502. DOI: 10.1126/science.1523409

63. Yuan L, Kaplowitz N. Glutathione in liver diseases and hepatotoxicity. Vol. 30, Molecular Aspects of Medicine. 2009. p. 29–41. DOI: 10.1016/j.mam.2008.08.003

64. Kaplowitz, N., Aw, TY., Ookhtens M. The Regulation of Hepatic Glutathione. Ann Rev Pharmacol Toxicol. 1985;25:715–44. DOI: 10.1146/annurev.pa.25.040185.003435

65. Akerboom TPM, Bilzen M, Sies H. The relationship of biliary glutathione disulfide efflux and intracellular glutathione disulfide content in perfused rat liver. J Biol Chem. 1982;257(8):4248–52. Available from: http://www.jbc.org/content/257/8/4248.long

66. Ballatori N, Krance SM, Notenboom S, Shi S, Tieu K, Hammond CL. Glutathione dysregulation and the etiology and progression of human diseases. Vol. 390, Biological Chemistry. 2009. p. 191–214. DOI: 10.1515/BC.2009.033

67. Forman HJ, Zhang H, Rinna A. Glutathione: Overview of its protective roles, measurement, and biosynthesis. Vol. 30, Molecular Aspects of Medicine. 2009. p. 1–12. DOI: 10.1016/j.mam.2008.08.006

68. Seelig GF, Simondsen RP, Meister A. Reversible dissociation of γ-glutamylcysteine synthetase into two subunits. J Biol Chem. 1984;259(15):9345–7. Available from: http://www.jbc.org/content/259/15/9345.long

69. Huang CS, Anderson ME, Meister A. Amino acid sequence and function of the light subunit of rat kidney gamma-glutamylcysteine synthetase. J Biol Chem. 1993;268(27):20578–83.

70. Huang CS, Chang L Sen, Anderson ME, Meister A. Catalytic and regulatory properties of the heavy subunit of rat kidney γ-glutamylcysteine synthetase. J Biol Chem. 1993;268(26):19675–80.

71. Oppenheimer L, Wellner VP, Griffith OW, Meister A. Glutathione synthetase. Purification from rat kidney and mapping of the substrate binding sites. J Biol Chem. 1979;254(12):5184–90. Available from: http://www.jbc.org/content/254/12/5184.long

72. Dalton TP, Chen Y, Schneider SN, Nebert DW, Shertzer HG. Genetically altered mice to evaluate glutathione homeostasis in health and disease. Vol. 37, Free Radical Biology and Medicine. 2004. p. 1511–26. DOI: 10.1016/j.freeradbiomed.2004.06.040

73. Grant CM, MacIver FH, Dawes IW. Glutathione is an essential metabolite required for resistance to oxidative stress in the yeast *Saccharomyces cerevisiae*. Curr Genet. 1996;29(6):511–5.

74. Shelly C. Lu MD. Glutathione Synthesis. Biochim Biophys Acta. 2013;1830(5):3143–53. DOI: 10.1016/j.bbagen.2012.09.008

75. Meister A, Anderson ME. Glutathione. Annu Rev Biochem. 1983;52:711–60.

76. Halliwell B. Free radicals, antioxidants, and human disease: Curiosity, cause, or consequence? Vol. 344, Lancet. 1994. p. 721–4. DOI: 10.1016/S0140-6736(94)92211-X

77. Takebe G, Yarimizu J, Saito Y, Hayashi T, Nakamura H, Yodoi J, et al. A comparative study on the hydroperoxide and thiol specificity of the glutathione peroxidase family and selenoprotein P. J Biol Chem. 2002;277(43):41254–8. DOI: 10.1074/jbc.M202773200

78. Deneke SM, Fanburg BL. Regulation of cellular glutathione. Am J Physiol. 1989;257(4 Pt 1):L163–73. DOI: 10.1152/ajplung.1989.257.4.L163

79. Liang CM, Lee N, Cattell D, Liang SM. Glutathione regulates interleukin-2 activity on cytotoxic T-cells. J Biol Chem. 1989;264(23):13519–23. Available from: http://www.jbc.org/content/264/23/13519.long

80. Suthanthiran M, Anderson ME, Sharma VK, Meister A. Glutathione regulates activation-dependent DNA synthesis in highly purified normal human T lymphocytes stimulated via the CD2 and CD3 antigens. Proc Natl Acad Sci. 1990;87(9):3343–7.

Available from: https://www.ncbi.nlm.nih.gov/pmc/articles/PMC53896/

81. Multhoff G, Meier T, C. B, M. W, Allenbacher A, Wilmanns W, *et al*. Differential Effects of Ifosfamide on the Capacity of Cytotoxic T Lymphocytes and Natural Killer Cells to Lyse Their Target Cells Correlate With Intracellular Glutathione Levels. Blood. 1995;85(8):2124–31.
Available from: http://www.bloodjournal.org/content/85/8/2124.long?sso-checked=true

82. Dröge W, Schulze-Osthoff K, Mihm S, Galter D, Schenk H, Eck HP, *et al*. Functions of glutathione and glutathione disulfide in immunology and immunopathology. FASEB J. 1994;8(14):1131–8.

83. Lewis AD, Hayes JD, Wolf CR. Glutathione and glutathione-dependent enzymes in ovarian adenocarcinoma cell lines derived from a patient before and after the onset of drug resistance: Intrinsic differences and cell cycle effects. Carcinogenesis. 1988;9(7):1283–7.

84. Mellish KJ, Kelland LR, Harrap KR. *In vitro* platinum drug chemosensitivity of human cervical squamous cell carcinoma cell lines with intrinsic and acquired resistance to cisplatin. Br J Cancer. 1993;68(2):240–50.

85. Godwin AK, Meister A, O'Dwyer PJ, Huang CS, Hamilton TC, Anderson ME. High resistance to cisplatin in human ovarian cancer cell lines is associated with marked increase of glutathione synthesis. Proc Natl Acad Sci U S A. 1992;89(7):3070–4.
Available from: https://www.ncbi.nlm.nih.gov/pmc/articles/PMC48805/

86. Griffith OW, Meister A. Potent and specific inhibition of glutathione synthesis by buthionine sulfoximine (S-n-butyl homocysteine sulfoximine). J Biol Chem. 1979;254(16):7558–60. Available from: http://www.jbc.org/content/254/16/7558.long

87. Sandor V, Flarakos T, Batist G, Wainer IW, Lloyd DK. Quantitation of the diastereoisomers of l-buthionine-(*R,S)*-sulfoximine in human plasma: a validated assay by capillary electrophoresis. J Chromatogr B Biomed Sci Appl. 1995;673(1):123–31.

88. Wainer IW. Drug Stereochemistry Analytical Methods and Pharmacology Clinical Pharmacology. Second Edition. 1993

89. Anderson CP, Tsai JM, Meek WE, Liu RM, Tang Y, Forman HJ, *et al*. Depletion of glutathione by buthionine sulfoximine is cytotoxic for human neuroblastoma cell lines via apoptosis. Exp Cell Res. 1999;246(1):183–92. DOI: 10.1006/excr.1998.4303

90. Campbell EB, Hayward ML, Griffith OW. Analytical and preparative separation of the diastereomers of l-buthionine-(*SR*)-sulfoximine, a potent inhibitor of glutathione biosynthesis. Anal Biochem. 1991;194(2):268–77. DOI: 10.1016/0003-2697(91)90229-M

91. Green J a, Vistica DT, Young RC, Hamilton TC, Rogan a M, Ozols RF. Potentiation of melphalan cytotoxicity in human ovarian cancer cell lines by glutathione depletion. Cancer Res. 1984;44(11):5427–31.
Available from: http://cancerres.aacrjournals.org/content/44/11/5427.long

92. Lewis AD, Durán GE, Lau DHM, Sikic BI. Sensitization of drug resistant human ovarian cancer cells to cyanomorpholino doxorubicin (MRA-CN) by modulation of glutathione metabolism. Int J Radiat Oncol Biol Phys. 1992;22(4):821–4.
Available from: https://linkinghub.elsevier.com/retrieve/pii/0360-3016(92)90532-M

93. Mistry P, Kelland LR, Abel G, Sidhar S, Harrap KR. The relationships between glutathione, glutathione-S-transferase and cytotoxicity of platinum drugs and melphalan in eight human ovarian carcinoma cell lines. Br J Cancer. 1991;64(2):215–20.
Available from: https://www.ncbi.nlm.nih.gov/pmc/articles/PMC1977519/

94. Bailey HH, Ripple G, Tutsch KD, Arzoomanian RZ, Alberti D, Feierabend C, *et al*. Phase

I study of continuous-infusion L-*S,R*-buthionine sulfoximine with intravenous melphalan. J Natl Cancer Inst. 1997;89(23):1789–96. DOI: 10.1093/jnci/89.23.1789

95. Gustafsson MGL, W J, Agard DA, Cited R, Examiner-thong P. United States Patent. R P Cargille Lab Inc. 1997. 3-6 p.

96. Khalafi L, Rafiee M, Fathi S. Effect of β-cyclodextrin on intra and intermolecular Michael addition of some catechol derivatives. Spectrochim Acta - Part A Mol Biomol Spectrosc. 2014;118:695–701. DOI: 10.1016/j.saa.2013.09.029

97. Sugiyama T, Kamura T, Kigawa J, Terakawa N, Kikuchi Y, Kita T, *et al*. Clinical characteristics of clear cell carcinoma of the ovary. Cancer. 2000;88(11):2584–9. DOI: 10.1002/1097-0142(20000601)88:11<2584::AID-CNCR22>3.0.CO;2-5

98. Otto Warburg B, Wind F, Negelein N. The Metabolism of tumors in the Body. The Journal of General Physiology. 1923;309(2):397–519.

99. Kleinman MH, Flory JH, Tomalia DA, Turro NJ. Effect of Protonation and PAMAM Dendrimer Size on the Complexation and Dynamic Mobility of 2-Naphthol. J Phys Chem B. 2000;104(48):11472–9. DOI: 10.1021/jp001882r

100. Wang Y, Wang L, Chen G, Gong S. Carboplatin-Complexed and cRGD-Conjugated Unimolecular Nanoparticles for Targeted Ovarian Cancer Therapy. Macromol Biosci. 2017;17(5):1–9. DOI: 10.1002/mabi.201600292

101. Madhusudhan A, Reddy GB, Venkatesham M, Veerabhadram G, Kumar AD, Natarajan S, *et al*. Efficient ph dependent drug delivery to target cancer cells by gold nanoparticles capped with carboxymethyl chitosan. Int J Mol Sci. 2014;15(5):8216–34. DOI: 10.3390/ijms15058216

102. Nematollahi D, Rafiee M, Fotouhi L. Mechanistic study of homogeneous reactions coupled with electrochemical oxidation of catechols. J Iran Chem Soc. 2009;6(3):448–76. Available from: https://link.springer.com/article/10.1007/BF03246523

103. Buglioni L, Bizet V, Bolm C. Methionine and buthionine sulfoximines: Syntheses under mild and safe imidation/oxidation conditions. Adv Synth Catal. 2014;356(10):2209–13. DOI: 10.1002/adsc.201400354

104. Jose S, U. Elsevier Science Publishers B . V., 1987. Elsevier Science Publishers B . V . 1987;44(85):305–16.

105. Campbell EB, Hayward ML, Griffith OW. Analytical and preparative separation of the diastereomers of L-buthionine-(*SR*)-sulfoximine, a potent inhibitor of glutathione biosynthesis. Analytical Biochemistry. 1991;194(2):268-77. DOI: 10.1016/0003-2697(91)90229-M

106. Kang MJ, Park SH, Kang MH, Park MJ, Choi YW. Folic acid-tethered pep-1 peptide-conjugated liposomal nanocarrier for enhanced intracellular drug delivery to cancer cells: Conformational characterization and *in vitro* cellular uptake evaluation. Int J Nanomedicine. 2013;8:1155–65. DOI: 10.2147/IJN.S39491

107. Kelemen LE. The role of folate receptor α in cancer development, progression and treatment: Cause, consequence or innocent bystander? Int J Cancer. 2006;119(2):243–50. DOI: 10.1002/ijc.21712

108. Elnakat H, Ratnam M. Distribution, functionality and gene regulation of folate receptor isoforms: Implications in targeted therapy. Adv Drug Deliv Rev. 2004;56(8):1067–84. DOI: 10.1016/j.addr.2004.01.001

109. Lu Y, Low PS. Folate-mediated delivery of macromolecular anticancer therapeutic agents.

Adv Drug Deliv Rev. 2012;64:342–52. DOI: 10.1016/j.addr.2012.09.020

110. Toffoli G, Russo A, Gallo A, Cernicoi C, Miotti S, Sorio R, *et al*. Expression of folate binding protein as a prognostic factor for response to platinum-containing chemotherapy and survival in human ovarian cancer. Int J Cancer. 1998;79(2):121–6. DOI: 10.1002/(SICI)1097-0215(19980417)79:2<121::AID-IJC4>3.0.CO;2-V

111. Yoo HS, Park TG. Folate receptor targeted biodegradable polymeric doxorubicin micelles. J Control Release. 2004;96(2):273–83. DOI: 10.1016/j.jconrel.2004.02.003

112. Leamon CP, Low PS. Folate-mediated targeting: From diagnostics to drug and gene delivery. Drug Discov Today. 2001;6(1):44–51. DOI: 10.1016/S1359-6446(00)01594-4

113. Zhao M-X, Huang H-F, Xia Q, Ji L-N, Mao Z-W. γ-Cyclodextrin–folate complex-functionalized quantum dots for tumor-targeting and site-specific labeling. J Mater Chem. 2011;21(28):10290. DOI: 10.1039/C1JM11066G

114. Low PS, Antony AC. Folate receptor-targeted drugs for cancer and inflammatory diseases. Adv Drug Deliv Rev. 2004;56(8):1055–8. DOI: 10.1016/j.addr.2004.02.003

115. Reddy JA, Dean D, Kennedy MD, Low PS. Optimization of folate-conjugated liposomal vectors for folate receptor- mediated gene therapy. J Pharm Sci. 1999;88(11):1112–8. DOI: 10.1021/js990169e

116. Chaudhury A, Das S, Bunte RM, Chiu GNC. Potent therapeutic activity of folate receptor-targeted liposomal carboplatin in the localized treatment of intraperitoneally grown human ovarian tumor xenograft. Int J Nanomedicine. 2012;7:739–51.

117. Fruehauf JP, Zonis S, Al-Bassam M, Kyshtoobayeva A, Dasgupta C, Milovanovic T, *et al*. Selective and Synergistic Activity of L-*S,R*-Buthionine Sulfoximine on Malignant Melanoma Is Accompanied by Decreased Expression of Glutathione-S-Transferase. Pigment Cell Res. 1997;10(4):236–49.

7. Appedix

7.1. Appendix I

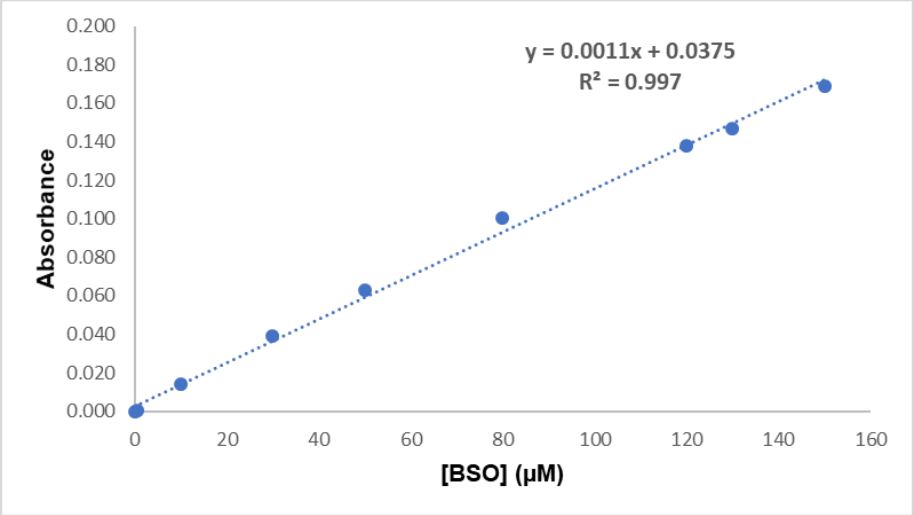

Figure 7.1 – Standard curve of derivate BSO measured at 503 nm.

7.2. Appendix II

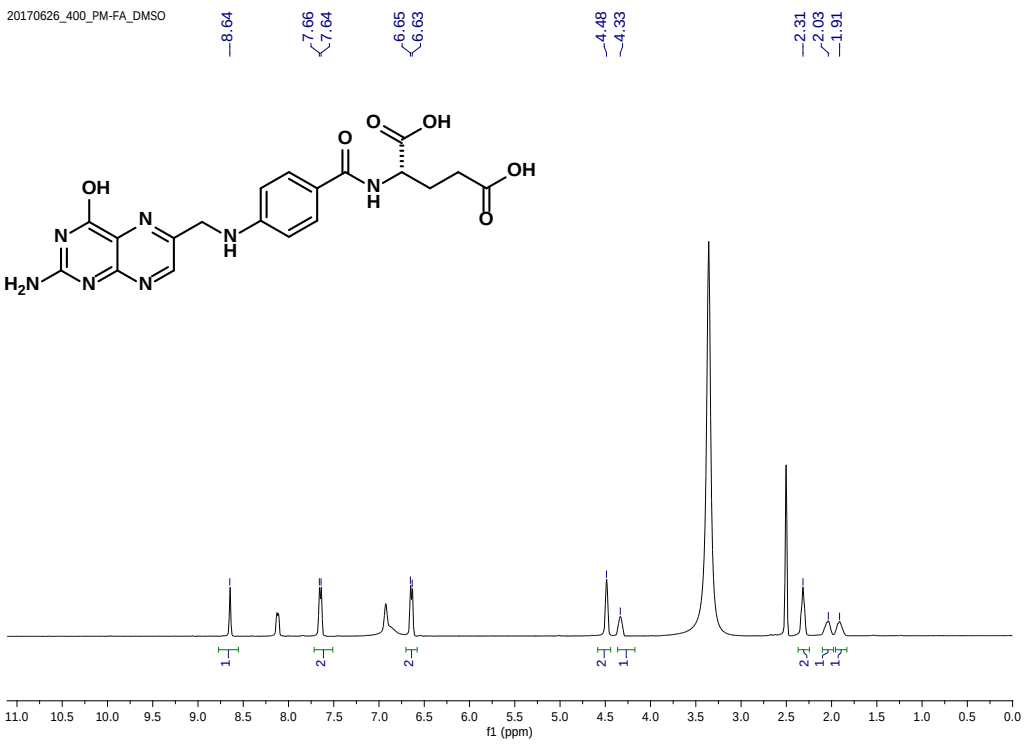

Figure 7.2 – ^{1}H NMR spectrum of folic acid (FA) in DMSO-*d6*.

7.3. Appendix III

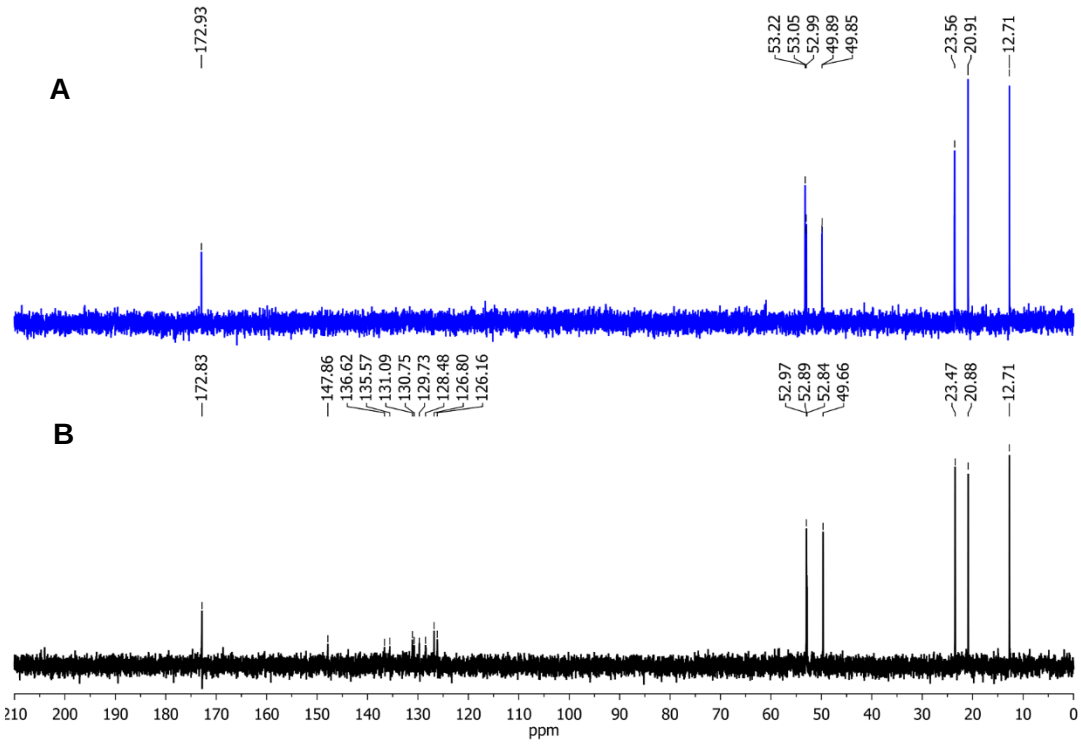

Figure 7.3 – ^{13}C NMR spectra of the BSO derivatization reaction. Comparative spectrum of (A) buthionine sulfoximine and (B) derivatization product.